

Chapter 8. Examination of Tsunami Wave Force Evaluations, Sediment Transport Calculations and Debris Impact Force

8.1. Tsunami wave force evaluation formula specifics

8.1.1. Evaluation formulae for tsunami wave force acting on maritime structures

(1) Evaluation formula for tsunami wave force acting on upright maritime structures

Formulae, which have previously been proposed, are presented below for assessing tsunami wave force acting on upright maritime structures.

1) Cases where soliton fission occurs

The impulsive tsunami wave force becomes larger when longwave tsunami head disperses into multiple shortwaves (soliton fission) developing bores-shaped waves. The evaluation formula presented by Ikeno et al. (2005) is the one that evaluates the corresponding tsunami wave force (modified Tanimoto formula).

The Ministry of Land, Infrastructure, Transport and Tourism (2013) presented conditions that take into account soliton fission based upon incident tsunami height and slope of sea bottom. Yasuda et al. (2006) stated that a sufficient propagation distance is required for soliton fission to develop. In addition to such knowledge, there are also methods that use analytical models capable of calculating soliton fission (one-dimensional analysis, etc.) to verify the presence of soliton fission.

[1]When water level at rear side of leading wave is higher than still water level

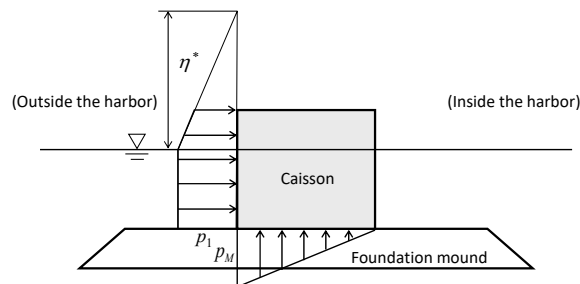
$$\begin{aligned}\eta^* &= 3.0a_I \\ p_1 &= 3.0\rho_0ga_I \\ p_M &= p_1\end{aligned}$$

where, η^* : tsunami wave pressure working height from the static water surface, a_I : height (amplitude) of incident tsunami from static water surface, ρ_0g : weight per unit volume of seawater, p_1 : tsunami wave pressure intensity on static water surface, and p_M : uplift pressure at upstanding wall front-side lower edge.

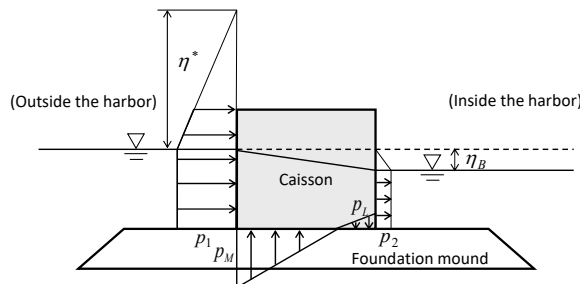
[2]When water level at rear side of leading wave is lower than still water level

$$\begin{aligned}\eta^* &= 3.0a_I \\ p_1 &= 3.0\rho_0ga_I \\ p_2 &= \rho_0g\eta_B \\ p_M &= p_1 \\ p_L &= p_2\end{aligned}$$

where, η^* : tsunami wave pressure working height from the static water surface, a_I : height (amplitude; numerical simulation results in the height of incident tsunami from static water surface a_I is $\frac{1}{2}$ of the tsunami height) of incident tsunami from static water surface, $\rho_0 g$: weight per unit volume of seawater, p_I : tsunami wave pressure intensity on static water surface, p_2 : negative pressure on outer surface of upstanding wall, p_M : uplift pressure at upstanding wall front-side lower edge, and p_L : uplift pressure at upstanding wall backside lower edge.



[1] When water level at rear side of leading wave is higher than still water level



[2] When water level at rear side of leading wave is lower than still water level

Figure 8.1.1-1 Schematic view of the evaluation formula presented by Ikeno et al. (2005)

2) Cases where soliton fission does not occur and does not overflow

If the water level fluctuates moderately, then it is possible to approximate hydrostatic pressure. However, even when soliton fission does not occur, tsunami wave force takes into consideration effect of shoaling waves and wave breaking. In such a case, the evaluation formula, which was presented by Tanimoto et al. (1984) (Tanimoto formula) and given in “Technical Standards and Accompanying Commentary for Port and Harbor Facilities” (Ports and Harbours Association of Japan, 2007), is applied to conditions where overflow does not occur.

[1]When water level at rear side of leading wave is higher than still water level

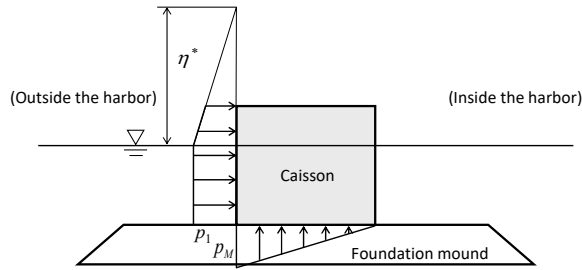
$$\begin{aligned}\eta^* &= 3.0a_I \\ p_1 &= 2.2\rho_0ga_I \\ p_M &= p_1\end{aligned}$$

where, η^* : tsunami wave pressure working height from the static water surface, a_I : height (amplitude; numerical simulation results in the height of incident tsunami from static water surface a_I is $\frac{1}{2}$ of the tsunami height) of incident tsunami from static water surface, ρ_0g : weight per unit volume of seawater, p_1 : tsunami wave pressure intensity on static water surface, p_M : uplift pressure at upstanding wall front-side lower edge, and p_L : uplift pressure at upstanding wall backside lower edge.

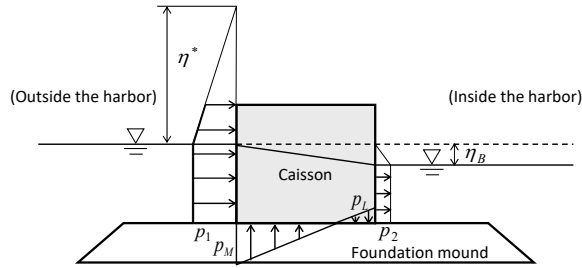
[2]When water level at rear side of leading wave is lower than still water level

$$\begin{aligned}\eta^* &= 3.0a_I \\ p_1 &= 2.2\rho_0ga_I \quad p_2 = \rho_0g\eta_B \\ p_M &= p_1 \quad p_L = p_2\end{aligned}$$

where, η^* : tsunami wave pressure working height from the static water surface, a_I : height (amplitude; numerical simulation results in the height of incident tsunami from static water surface a_I is $\frac{1}{2}$ of the tsunami height) of incident tsunami from static water surface, ρ_0g : weight per unit volume of seawater, p_1 : tsunami wave pressure intensity on static water surface, p_2 : negative pressure on outer surface of upstanding wall, p_M : uplift pressure at upstanding wall front-side lower edge, and p_L : uplift pressure at upstanding wall backside lower edge.



[1] When water level at rear side of leading wave is higher than still water level



[2] When water level at rear side of leading wave is lower than still water level

Figure 8.1.1-2 Schematic view of the evaluation formula presented by Tanimoto et al. (1984)

3) Cases where soliton fission does not occur but overflow does

If soliton fission does not occur and overflow does occur, the evaluation formula, which is presented in “Tsunami-Resistant Design Guideline for Breakwaters” (Ministry of Land, Infrastructure, Transport and Tourism, 2013), is applied that has been corrected for the hydrostatic pressure difference (maximum water level difference) acting on the front and back sides of the target structure.

If an evaluation formula is applied that is based upon hydrostatic pressure difference in a state where there is slight overflow, it is possible that applying the Tanimoto formula in a state where there is overflow immediately in front of where the water level is even lower may result in significant tsunami wave force, so both are compared and the greater value adopted.

$$p_1 = a_f \rho_0 g (\eta_f + h')$$

$$p_2 = \frac{\eta_f - h_c}{\eta_f + h'} p_1$$

$$p_3 = a_r \rho_0 g (\eta_r + h')$$

where, p_1 : tsunami wave pressure intensity on front-side bottom of upstanding wall, p_2 : tsunami wave pressure intensity on front-side top of upstanding wall, p_3 : tsunami wave pressure intensity on backside bottom of upstanding wall, $\rho_0 g$: weight per unit volume of seawater, h' : water depth at bottom surface of upstanding wall, h_c : height from static water surface to top of upstanding wall, η_f : tsunami height from static water surface in front-side of upstanding wall, a_f : hydrostatic pressure correction coefficient in front-side of upstanding wall based on

hydraulic model experiment results ($=1.05$), and a_r : hydrostatic pressure correction coefficient behind upstanding wall based on hydraulic model experiment results ($=0.9$).

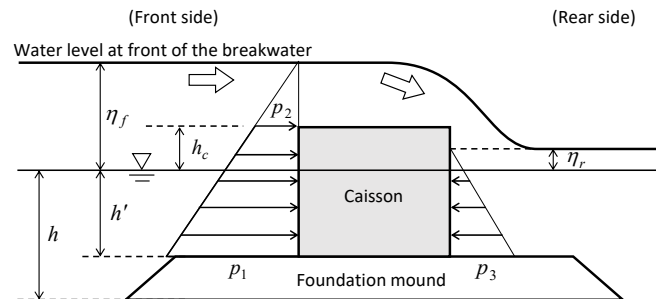


Figure 8.1.1-3 Schematic view of the evaluation formula presented by Ministry of Land, Infrastructure, Transport and Tourism (2013)

(2) Formulae for assessing tsunami wave force acting on sloped maritime structures

Based upon Mizutani and Imamura (2000) and Mizutani and Imamura (2002), the tsunami wave force acting on sloped maritime structures is classified as described below in accordance with the conditions in which such force occurs.

- Hydro dynamic pressure and impulsive hydro dynamic pressure: These develop on the moment when incident tsunami strikes a structure. Impulsive hydro dynamic pressure is largely related to the slope in front of the structure and there is a high probability of impulsive hydro dynamic pressure developing when the slope is almost vertical if not completely.
- Run-up pressure: After the strike of an incident tsunami, run-up pressure develops when the water level rises significantly as waves continue to arrive.
- Impact continuous pressure and impulsive impact continuous pressure: These develop instantaneously as the result of the strike of reflective tsunami and incident tsunami. When the dimensionless value $\Delta p/\rho g H$ is 2.0 or greater based on the wave height for the difference with run-up pressure, this is referred to as impulsive impact continuous pressure.
- Overflow pressure and impulsive overflow pressure: These develop due to a tsunami that overflows a sloped structure. If the flow velocity at crest and rear slope angle are high, the overflow pressure increases and impulsivity increases.

For each of the aforementioned classifications, formulae, which have previously been proposed, are given below for assessing tsunami wave force acting on sloped maritime structures.

- 1) Hydro dynamic pressure and impulsive hydro dynamic pressure (Fukui et al., 1962; Mizutani and Imamura, 2000; Mizutani and Imamura, 2002)

$$p_d(z) = p_{dm} \left(1 - 1.4 \frac{z}{R} \right) \quad \left(\frac{z}{R} \geq 0 \right) ; \text{ Above the static water surface}$$

(Fukui et al., 1962)

$$p_d(z) = p_{dm} \left(1 - \frac{z}{R} \right)^3 \quad \left(\frac{z}{R} \geq 0 \right) ; \text{ Above the static water surface}$$

(Mizutani and Imamura, 2000)

$$p_d(z) = p_{dm} \left(1 + \frac{z}{2R} \right) \quad \left(\frac{z}{R} \leq 0 \right) ; \text{ Below the static water surface}$$

(both of the above references)

where, p_d : hydro dynamic pressure distribution, R : run-up height, and z : positive coordinates upward from the static water surface. Also, p_{dm} is the hydro dynamic pressure or impulsive hydro dynamic pressure, and it is calculated using wave velocity c according to the following equation.

$$p_{dm} = 0.12 \frac{wc^4}{g^2H} ; \text{ Hydro dynamic pressure (Mizutani and Imamura, 2000)}$$

$$p_{dm} = 0.25 \frac{wc^4}{g^2H} ; \text{ Impulsive hydro dynamic pressure (Mizutani and Imamura, 2002)}$$

$$c = \sqrt{\frac{g(H+h)(H+2h)}{2(H+h-\eta \cdot H)}}$$

where, w : weight per unit volume of water, h : water depth, η : resistance coefficient (Fukui et al., 1962) and H : incident wave height. Also, the conditions for development of impulsive hydro dynamic pressure are shown in the following equation using dip-slope angle θ_I in the structure front-side.

$$\frac{c^2}{gH} \leq -0.6 \cot \theta_I + 3.45$$

2) Run-up pressure (Mizutani and Imamura, 2000)

$$p_{sm} = 0.14(2 + \cos \theta_I) \cdot p_{dm} \frac{c^2}{gH} \quad (0 < \cos \theta_I < 0.71)$$

$$p_{sm} = 0.38 p_{dm} \frac{c^2}{gH} \quad (0.71 < \cos \theta_I)$$

where, p_{sm} : maximum sustained tsunami wave pressure, p_{dm} : hydro dynamic pressure, θ_I : dip-slope angle in the structure front-side, c : bore wave velocity, and H : incident wave height. Also, sustained tsunami wave pressure distribution p_s is expressed with the following equation.

$$p_s(z) = p_{sm} \left(1 - 2.5 \frac{z}{R} \right) \quad \left(\frac{z}{R} \geq 0 \right) ; \text{ Above the static water surface}$$

$$p_s(z) = p_{sm} \left(1 + \frac{z}{3R} \right) \quad \left(\frac{z}{R} \leq 0 \right); \text{ Below the static water surface}$$

where, R : run-up height and z : positive coordinates upward from the static water surface.

3) Impact continuous pressure (Mizutani and Imamura, 2000)

- Case where the dip-slope angle θ_l in front of the structure is comparatively steep

$$p_{im} = 0.5(p_{dm} + p_{sm}) \quad (h \cot \theta_l \leq 0.15m)$$

where, p_{im} : maximum impact continuous pressure, p_{sm} : maximum sustained tsunami wave pressure, p_{dm} : hydro dynamic pressure, and h : water depth. Also, the impact tsunami wave pressure distribution p_i is expressed with the following equation.

$$p_i(z) = p_{im} \left(0.9 - 3 \frac{z}{R} \right) \quad \left(\frac{z}{R} \geq 0 \right); \text{ Above the static water surface}$$

$$p_i(z) = 0.9 p_{im} \quad \left(\frac{z}{R} \leq 0 \right); \text{ Below the static water surface}$$

where, R : run-up height and z : positive coordinates upward from the static water surface.

- Case where the dip-slope angle θ_l in front of the structure is 45 degrees or less and the static water depth is deep

$$p_{im} = 0.5(p_{dm} + p_{sm}) + 2200 \quad (0.15m > h \cot \theta_l)$$

where, p_{im} : maximum impact continuous pressure, p_{sm} : maximum sustained tsunami wave pressure, p_{dm} : hydro dynamic pressure, and h : water depth. Also, the impact continuous pressure distribution p_i is expressed with the following equation.

$$p_i(z) = p_{im} \left(2 - 10 \frac{z}{R} \right) \quad \left(\frac{z}{R} \geq 0.1 \right); \text{ Above the static water surface}$$

$$p_i(z) = p_{im} \left(0.35 + 6.5 \frac{z}{R} \right) \quad \left(0 \leq \frac{z}{R} \leq 0.1 \right); \text{ On the static water surface}$$

$$p_i(z) = 0.35 p_{im} \quad \left(\frac{z}{R} \leq 0 \right); \text{ Below the static water surface}$$

where, R : run-up height and z : positive coordinates upward from the static water surface.

4) Overflow pressure and impulsive overflow pressure (Mizutani and Imamura, 2002)

$$\frac{p_{om}}{\rho g H_{d2}} = 2\sqrt{2} \frac{V_m \sin \theta_2}{\sqrt{g H_{d2}}} \quad ; \text{ Overflow pressure}$$

$$\frac{p_{om}}{\rho g H_{d2}} = \left(2\sqrt{2} \frac{V_m \sin \theta_2}{\sqrt{g H_{d2}}} \right)^4 \quad ; \text{ Impulsive overflow pressure}$$

where, p_{om} : maximum overflow pressure, H_{d2} : rear surface height, V_m : maximum flow velocity at crest, and θ_2 : rear surface slope angle. Also, the maximum overflow pressure p_{om} is expressed with the following equation.

$$p_{om} = A\rho V_m \sqrt{2gH_{d2}} \sin \theta_2$$

where, A : coefficient determined empirically, and ρ : water density. Also, the conditions for development of impulsive overflow pressure are given with the following equation.

$$2\sqrt{2} \frac{V_m \sin \theta_2}{\sqrt{gH_{d2}}} \geq 1$$

8.1.2. Evaluation formula for tsunami wave force acting on land structures

The formulae for assessing tsunami wave force acting on land structures may be classified into evaluation formulae using hydraulic quantity not affected by the structure, which is obtained by means of a tsunami run-up calculation without the structure subject to evaluation, and evaluation formulae using hydraulic quantity affected by the structure which is obtained by means of a tsunami run-up calculation that takes into account the target structure. The previously proposed formulae for assessing tsunami wave force acting on land structures are shown below according to this classification.

(1) Evaluation formulae based on hydraulic quantity in a state without a structure

1) Evaluation formula using maximum inundation depth

For the evaluation formula based on hydraulic quantity in a state without a target structure, and evaluation formula that regards tsunami wave pressure as a hydrostatic pressure equivalent to three times the maximum inundation depth of a progressive wave (Asakura et al., 2000) has generally been used widely, and also referenced in the guidelines for tsunami evacuation buildings (Cabinet Office, 2005).

$$p_{\max}(z) = \rho g (\alpha h_{i\max} - z)$$

where, z is the height from the ground surface, ρ is the fluid density, g is the gravitational acceleration, and $h_{i\max}$ is the maximum inundation depth of a progressive wave in a state without structures. α is the water depth coefficient, and $\alpha = 3.0$ when the Froude number, which is calculated using the maximum inundation depth and maximum flow velocity, is 1.5 or greater, and $\alpha = 1.0$ when the Froude number is close to 1.0 (hydrostatic pressure), but $\alpha = 3.0$ has been proposed as a value capable of enveloping all data.

The National Institute for Land and Infrastructure Management (2012) proposed a reduction in the Asakura et al. (2000) water depth coefficient dependent upon the distance from the coastline and the presence of shielding, which was based on the results of a consolidation using the Froude number for field data.

On the other hand, Sakakiyama (2012) and Ishida et al. (2014) confirmed based upon hydraulic model experiment and analysis, when the Froude number exceeds 1.5, the water

depth coefficient α exceeds 3, and it is desirable to appropriately set the water depth coefficient α in keeping with the Froude number.

Also, Ikeno et al. (2006) proposed the following formula because the results of hydraulic model experiment simulating soliton fission waves showed that, when the run-up water depth is lower, the overflow water mass surges higher when the wave strikes a land structure and the water depth coefficient α is relatively great.

- Main tsunami wave pressure P_1

$$P_1(z)/(\rho g \eta_{\max}) = -z/\eta_{\max} + \alpha$$

- Soliton fission wave predominant portion tsunami wave pressure P_2

$$P_2(z)/(\rho g \eta_{\max}) = K_1(-z/(K_2 \eta_{\max}) + \alpha)$$

- Acting tsunami wave pressure P

$$P(z) = \max(P_1(z), P_2(z))$$

$$\alpha = 1.35/(\eta_{\max}/h) + 1.5 \quad ; 0.3 \leq \eta_{\max}/h \leq 0.9$$

$$K_1 = 1.8, \quad K_2 = 1.35/\alpha$$

where, z : height from the ground surface, ρ : fluid density, g : gravitational acceleration, η_{\max} : maximum amplitude of level of progressive wave at structure location, α : water depth coefficient, and h : water depth in front of revetment, and the tsunami wave pressure of the main tsunami wave is calculated using P_1 , and the difference between P_1 and P_2 is added if there is action of the soliton fission wave.

Cabinet Office (2005) stated that of the tsunami wave pressures in a triangular distribution based upon Asakura et al. (2000) when tsunami overflows a structure, the trapezoidal distribution acts up to the height where a structure is present. By contrast, the Fire and Disaster Management Agency (2009) proposed, based upon hydraulic model experiments and an examination using CADMAS-SURF, a formula that reduces the tsunami wave pressure acting on the bottom surface in accordance with the ratio of inundation depth to oil weir height.

$$P_{\max} = (1 + \alpha_d) \rho g \eta_{\max}$$

$$\alpha_d = \begin{cases} -0.692(h_c/\eta_{\max})^2 + 2.352(h_c/\eta_{\max}) & (h_c/\eta_{\max} \leq 1.7) \\ 2.0 & (h_c/\eta_{\max} > 1.7) \end{cases}$$

where, h_c : oil weir height, η_{\max} : maximum inundation depth of progressive wave, and α_d : dynamic pressure coefficient.

2) Evaluation formula using maximum inundation depth and flow velocity

- Hydrostatic pressure-type evaluation formula

Asakura et al. (2002) consolidated empirical data on cross-sectional two-dimensional structures and three-dimensional structures, and took into account the effect of flow velocity by regarding the factor α in Asakura et al. (2000) as a function of the Froude number.

$$\alpha = 1.2F_r + 1.0$$

where, Froude number F_r is calculated according to the following formula using the maximum inundation depth η_{max} and flow velocity u_η at the time such inundation occurs.

$$Fr = u_\eta / \sqrt{g\eta_{max}}$$

Sakakiyama (2012) arranged the factor α in Asakura et al. (2000) as a function of the Froude number based upon numerical simulations of cross-sectional two-dimensional structures. The Froude number F_r is defined the same as in Asakura et al. (2002).

$$\alpha = 1.4F_r + 1.0$$

- Drag-type evaluation formula

Omori et al. (2000) evaluated tsunami wave force in the time series based upon the modified Morison equation.

$$F_H = \frac{1}{2}\rho C_D u |u| B \eta + \rho C_M \dot{u} B L \eta + \frac{1}{2}\rho C_S(\theta) u |u| B \eta + \rho g B L \eta \frac{d\eta}{dx}$$

where, C_D : drag coefficient (=2.05), C_M : inertial force coefficient (=2.19), C_S : impact force coefficient (=3.6tan θ , θ : wave surface angle), u : horizontal flow velocity of tsunami progressive wave, \dot{u} : horizontal acceleration of tsunami progressive wave, η : inundation depth due to tsunami progressive wave, B : structure width, and L : structure length. The right-hand side first term is the term for drag, right-hand side second term is the term for inertial force, right-hand side third term is the term for impact force, and right-hand side fourth term is the term for the hydraulic gradient force.

- Evaluation formula for tanks

The Fire and Disaster Management Agency (2009) proposed a method for outdoor storage tanks which calculates the tsunami wave force using maximum inundation depth and maximum flow velocity in a state where an oil weir is present but there are no tanks.

Horizontal tsunami wave force F_{dH}

$$F_{dH} = \frac{1}{2} \int_{-\pi}^{\pi} \rho g [h_x^{\max}(\theta)]^2 R \cos \theta d\theta$$

$$h_x^{\max}(\theta) = \alpha \eta_{\max} \sum_{m=0}^3 p_m \cos m\theta$$

$$p_0 = 0.680, \quad p_1 = 0.340, \quad p_2 = 0.015, \quad p_3 = -0.035$$

where, α : inundation depth coefficient related to horizontal tsunami wave force (1.8 according to previous reviews) uses the value in the following formula according to the Froude number found based on maximum inundation depth and maximum flow velocity in a state where no tanks have been set up.

$$\alpha = \begin{cases} 1.8 & (F_r \geq 1.3) \\ 2.0F_r - 0.8 & (1.3 \geq F_r \geq 0.9) \\ 1.0 & (0.9 \geq F_r) \end{cases}$$

Vertical tsunami wave force F_{IV}

$$F_{IV} = 2 \int_0^\pi \rho g h_V^{\max}(\theta) R^2 \cos^2 \theta d\theta$$

$$h_V^{\max}(\theta) = \beta \eta_{\max} \sum_{m=0}^3 q_m \cos m\theta$$

$$q_0 = 0.720, \quad q_1 = 0.308, \quad q_2 = 0.014, \quad q_3 = -0.042$$

where, β : inundation depth coefficient related to vertical tsunami wave force uses the value in the following formula according to the Froude number found based on maximum inundation depth and maximum flow velocity in a state where no tanks have been set up.

$$\beta = \begin{cases} 1.2 & (F_r \geq 1.3) \\ 0.5F_r + 0.55 & (1.3 \geq F_r \geq 0.9) \\ 1.0 & (0.9 \geq F_r) \end{cases}$$

(2) Evaluation formulae based on hydraulic quantity in a state with a structure

1) Evaluation formula using inundation depth in front of structure

Iizuka and Matsutomi (2000) proposed an evaluation formula that uses inundation depth in front of structure.

$$F_D = \frac{1}{2} \rho C_D u^2 A = \frac{1}{2} \rho C_D u^2 h_f B = 0.61 \gamma_w C_D h_f^2 B$$

where, C_D : drag coefficient, u : flow velocity on land, A : structure inundation area, h_f : inundation depth in front of the structure, B : structure width, and γ_w : weight per unit volume of fluid.

2) Evaluation formula using inundation depth and flow velocity in front of structure

Arimitsu et al. (2012) proposed the following formula for finding the time series of the tsunami wave pressure vertical distribution by using inundation depth and flow velocity in front of the structure.

$$p(z, t) = \rho g \{h_f(t) - z\} + \rho u_f(t)^2$$

where, ρ : fluid density, g : gravitational acceleration, z : action location, and t : time.

The aforementioned formula is the distribution of hydrostatic pressure according to inundation depth h_f in front of the structure when a structure is present and the pressure, which is in keeping with the horizontal flow velocity u_f based upon the law of conservation of momentum, is acting upon the structure.

- 3) Evaluation formula using inundation depth and flow velocity in the offing at a distance of five times the tsunami depth from the structure

Kihara et al. (2012) and Takabatake et al. (2013) focused on structures having a width equivalent to between 0.5 to 5 times the depth of inflow, and proposed the following formula which uses inundation depth and flow velocity in the offing at a distance of five times the depth of the inflowing tsunami from the structure.

$$F = \frac{1}{2} \rho g \left(h_{in} + \frac{u_{in}^2}{2g} \right)^2 W, p = \rho g \left(h_{in} + \frac{u_{in}^2}{2g} - z \right)$$

where, h_{in} and u_{in} : inundation depth and flow velocity at a point that is five times a representative inflowing tsunami depth in an upstream direction from the target structure, and W : structure width.

- (3) Hydraulic quantity used in calculation of tsunami wave force

Sections (1) and (2) present formulae for assessing tsunami wave force acting on land structures that are separated into cases where hydraulic quantity is used in a state where there are no structures and hydraulic quantity in a state where there are structures present. In addition, the hydraulic quantities used may be classified into cases where only inundation depth is used and cases where both inundation depth and flow velocity are used.

The maximum inundation depth used in evaluation formulae presented by Asakura et al. (2000), Cabinet Office (2005), and the Ministry of Land, Infrastructure, Transport and Tourism (2012) is the maximum inundation depth of a progressive wave that does not include the effect of reflection from land. Also, the evaluation formula presented by Iizuka and Matsutomi (2000) uses the inundation depth in front of the structure.

The evaluation formulae presented by Asakura et al. (2002) and Sakakiyama (2012) used the maximum inundation depth of a progressive wave as well as the Froude number found from the maximum inundation depth and the flow velocity at the time the maximum inundation depth occurs. The Fire and Disaster Management Agency (2009) also used the maximum inundation depth and the Froude number. However, for calculating the Froude number, the Fire and Disaster Management Agency (2009) used the maximum inundation depth and maximum flow velocity when the occurrence times are different.

The evaluation formulae presented by Omori et al. (2000), Arimitsu et al. (2012), Kihara et al. (2012), and Takabatake et al. (2013) used the time series of inundation depth and flow velocity.

- (4) Classification of tsunami wave pressure

Arikawa et al. (2005) classified the tsunami wave pressure acting on an upstanding wall according to the time series (see Main Volume Section 6.5.2). The evaluation formulae presented

by Omori et al. (2000) and Arimitsu et al. (2012) take into account impulsive hydro dynamic pressure positively, and it is possible to calculate both hydro dynamic pressure and continuous pressure. On the other hand, the evaluation formulae presented by Iizuka and Matsutomi (2000), Kihara et al. (2012), and Takabatake et al. (2013) focused only continuous pressure. The evaluation formulae presented by Asakura et al. (2000), Cabinet Office (2005), Ministry of Land, Infrastructure, Transport and Tourism (2012), Fire and Disaster Management Agency (2009), Asakura et al. (2002), and Sakakiyama (2012) arrange maximum tsunami wave force and tsunami wave pressure without regard to causal factors, and the proposed equations comprised both impulsive hydro dynamic pressure and maximum continuous pressure.

(5) Shape of target structure

Structure shapes may be classified into three-dimensional structures such as buildings in which a tsunami flows into the structure to the back through sides of the structure, and two-dimensional structures such as seawalls that are uniform in a cross direction and the tsunami does not flow through to the back with the exception of overflow.

The evaluation formulae presented by Asakura et al. (2000), Sakakiyama (2012), and Takabatake et al. (2013) focused on two-dimensional structures where the tsunami does not wrap around the sides. The Fire and Disaster Management Agency (2009) formula for assessing tsunami wave force acting on oil weirs has also been reviewed using vertical two-dimensional calculations. The focus of the evaluation formulae presented by the Cabinet Office (2005) and the Ministry of Land, Infrastructure, Transport and Tourism (2012) are three-dimensional structures. The evaluation formulae presented by Omori et al. (2000) and Iizuka and Matsutomi (2000) focused on three-dimensional structures, and the focus of the Fire and Disaster Management Agency (2009) formula for assessing tsunami wave force acting outdoor storage tanks was a three-dimensional structure. Kihara et al. (2012) focused on three-dimensional structures having a width equivalent to between 0.5 and 5 times the inflow depth. Asakura et al. (2002) and Arimitsu et al. (2012) focused on both two-dimensional structures and three-dimensional structures.

8.1.3. Examples of tsunami wave force acting on the ground in the vicinity of structures, etc.

8.1.3.1. Simplified calculation method for pressure acting on ground surface as presented by Omura et al. (2014)

Omura et al. (2014) used a simplified calculation to find the pressure acting on the ground surface behind a seawall when a tsunami overflows the seawall and falls to the ground surface.

The simplified calculation regards the horizontal flow velocity v_x of the portion overflowing the seawall as $(gh)^{0.5}$ (h is the overflow depth, and g is the gravitational acceleration), and the overflow motion is assumed to be a parabolic drop motion to find the flow velocity v , strike angle θ , and overtopping wave distance s , and using these as conditions, calculates the maximum hydro dynamic pressure p_d without a water cushion following the evaluation of dynamic pressure of the freefall-type energy dissipater for a dam (Japan Society of Civil Engineers, 1971).

$$\frac{p_d}{\rho g} = \frac{(v \sin \theta)^2}{2g}$$

$$s = v_x t \quad , \quad v = \sqrt{v_x^2 + v_z^2} \quad , \quad \theta = \tan^{-1}(v_z/v_x)$$

$$v_x = \sqrt{gh} \quad , \quad v_z = gt \quad , \quad t = \sqrt{\frac{2(H + 0.5h)}{g}}$$

where, ρ : water density, v_x : horizontal flow velocity, v_z : vertical flow velocity, t : time, and H : height of seawall.

8.1.3.2. Simplified estimation method for overflow routes, etc. as presented by Mitsui et al. (2015)

(1) Simplified estimation method for overflow routes

Mitsui et al. (2015) presented the following simplified method for estimating overflow routes of tsunami overflowing a breakwater.

- Caisson dimensions and tsunami height are already known. (Figure 8.1.3.2-1).
- The calculation diagram presented by Mitsui et al. (2015) is used to read flow rate coefficient m , h_2/h_1 , and u_{2z}/u_{2x} .
- Water route thickness h_2 at the caisson heel is found based on the read h_2/h_1 , and flow velocities u_{2x} and u_{2z} may be calculated using the following formula.

$$u_{2x} = q/h_2, \quad q = mh_1\sqrt{2gh_1}$$

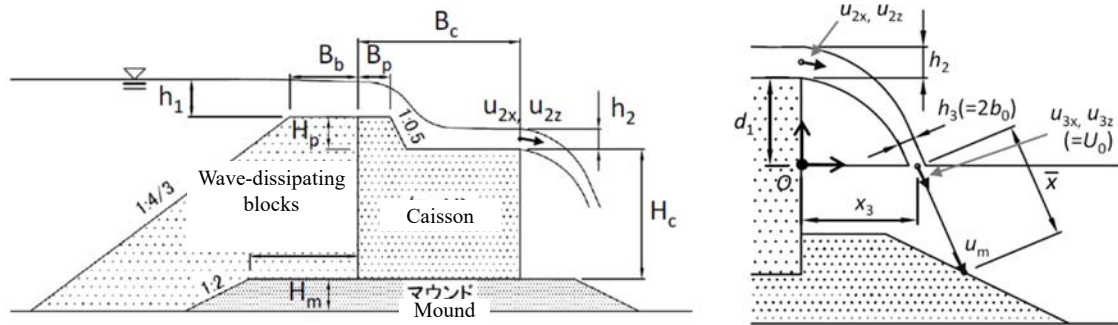
- The trajectory of the overflow route assumed that water particles fall freely from the caisson heel, and flow velocities u_{3x} and u_{3z} as well as water landing location x_3 are determined as shown below.

$$u_{3x} = u_{2x}, \quad u_{3z} = -\sqrt{u_{2z}^2 + 2g(d_1 + h_2/2)}, \quad x_3 = u_{2x} \frac{u_{2z} + \sqrt{u_{2z}^2 + 2g(d_1 + h_2/2)}}{g}$$

- The route thickness h_3 at the water landing location is determined using the following formula, and the trajectory under the water surface inside the port is assumed to be a straight line.

$$h_3 = q / \sqrt{u_{3x}^2 + u_{3z}^2}$$

Mitsui et al. (2015) used the aforementioned simplified estimation method to calculate the route trajectory, and stated that, for the most part, the empirical results, numerical analysis results, and results using the simplified estimation method coincide.



(Left side: Sectional view of breakwater, Right side: Trajectory of the overflow nappe)

Figure 8.1.3-1 Size definition of an estimation method for the trajectory of the overflow nappe proposed by Mitsui et al. (2015)

(2) Method for estimating driving flow velocity

Mitsui et al. (2015) also presented a method for estimating the driving flow velocity towards mounds inside a port. The results presented by Mitsui et al. (2015) stated that good estimation results were able to be obtained for the most part when $C_1=3.0$. The method for estimating driving flow velocity is described below.

- Based upon flow velocity U_0 for the overflow route on the water surface inside the port, the flow velocity driving toward mounds inside the port is estimated.
- Rajaratnam (1976) presented the following formula based on a theoretical solution and previous empirical results for flow velocity at the central axis of a two-dimensional water jet spouting from a nozzle.

$$u_m/U_0 = C_1/\sqrt{\bar{x}/b_0}, \quad C_1 = 3.5$$

where, U_0 is the flow velocity at the exhaust nozzle, u_m the flow velocity on the central axis, b_0 : 1/2 of the exhaust nozzle width, \bar{x} : the distance from exhaust nozzle, and C_1 : the empirical constant.

- When this is applied to the overflow route and considered, U_0 is the absolute value of the flow velocity at the location of the water surface inside the port, $2b_0$ is the route thickness on the water surface, \bar{x} is the distance from the water landing location to the mound driving location, and the flow velocity u_m driving towards the mound is determined based upon the relationship in the aforementioned formula.

For the experiment, a model of a seawall was set up, which was 1.5 m high and 4.0 m wide, near the center of the water channel, and measurements of the inundation depth, flow velocity, and pressure were taken for seven (Cases 1 through 7) tsunami shapes having different inundation depths and flow velocities upstream of the seawall. Figure 8.1.4-2 shows the inundation depths upstream of the seawall, flow velocity, and Froude number time series tsunami shapes.

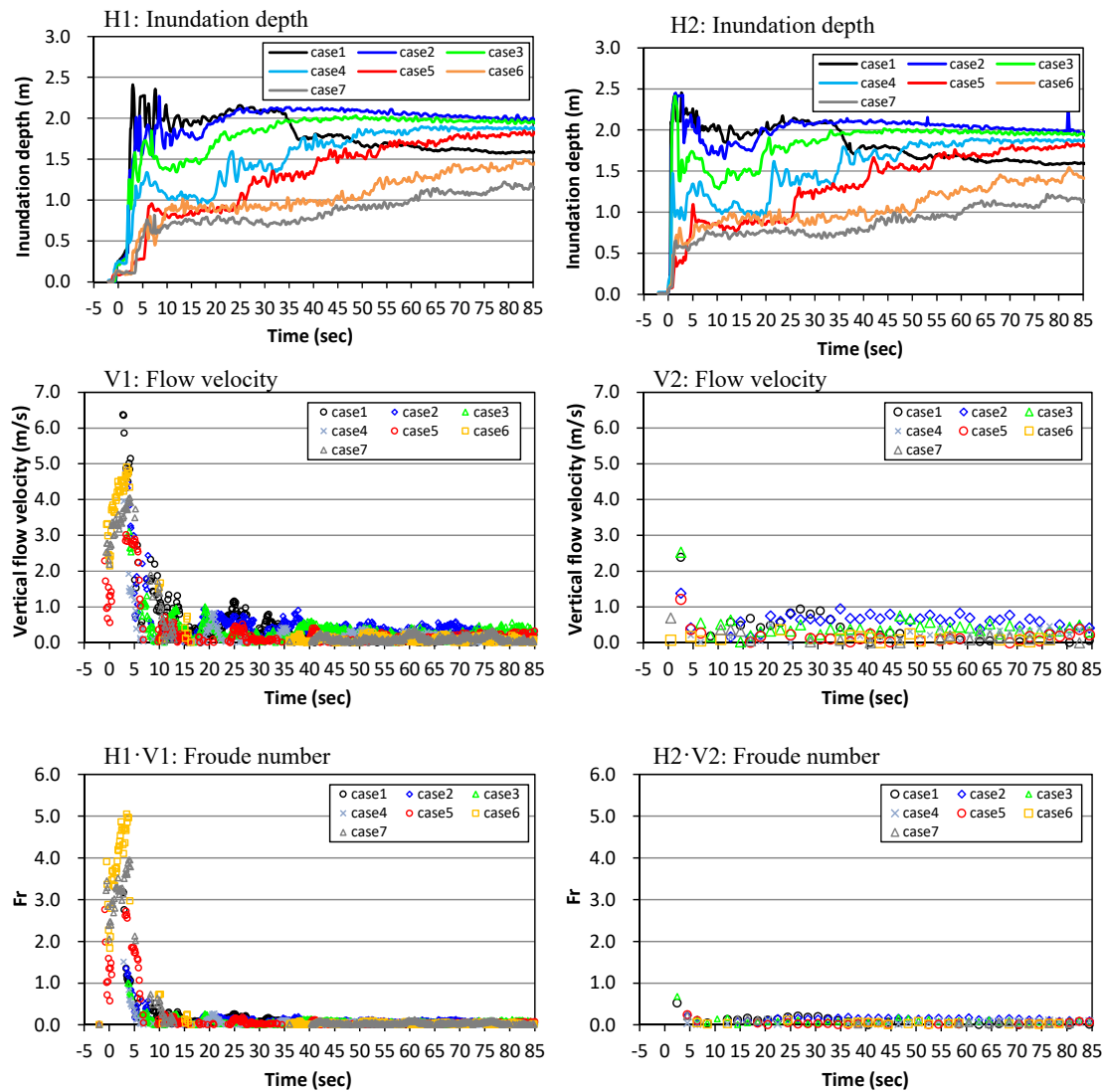


Figure 8.1.4-2 Time series of inundation depth upstream of the seawall, flow velocity, and Froude number

(2) Tsunami wave force calculation methods

Tsunami wave force evaluation formulae used for comparison with empirical results are given below. The most appropriate positional data was selected from among the geodetic points

for the empirical inundation depths and flow velocities used in the calculation of tsunami wave force.

- 1) Tsunami wave force evaluation formula using hydraulic quantity in a state without structures
 - Tsunami wave force evaluation formula presented by Asakura et al. (2000) (water depth coefficient $\alpha=3.0$)

Since the maximum inundation depth of the progressive wave was not measured in the experiment, the maximum inundation depth at point H2 where the structure exists was used 0.5 times for the stability of the tsunami wave force assuming the condition of perfect reflection.

- 2) Tsunami wave force evaluation formula using hydraulic quantity in a state with structures
 - Tsunami wave force evaluation formula presented by Arimitsu et al. (2012)

To calculate the tsunami wave force, the empirical results were used for inundation depth and flow velocity at points H2 and V2.
 - Tsunami wave force evaluation formula presented by Takabatake et al. (2013)

To calculate the tsunami wave force, the empirical results were used for inundation depth and flow velocity at points H1 and V1.

(3) Results of tsunami wave force calculations

- 1) Tsunami wave force evaluation formula using hydraulic quantity in a state without structures

Figure 8.1.4-3 is a comparison of the maximum tsunami wave pressures as measured by tsunami wave pressure meters in experiments and the maximum tsunami wave pressure according to the evaluation formula presented by Asakura et al. (2000). In all of the cases as well, the maximum tsunami wave pressure according to the evaluation formula presented by Asakura et al. (2000) was approximately 1.5 times the empirical results, obtaining results that sufficiently encompass the empirical results.

- 2) Tsunami wave force evaluation formula using hydraulic quantity in a state with structures

Figure 8.1.4-4 shows the empirical results of a tsunami wave force time series acting on a seawall and the results of calculations using tsunami wave force evaluation formulae. The features are shown below of each tsunami wave force evaluation formula, which have been obtained from the results of comparisons of these formulae.

 - In a quasi-steady state ($t \geq 10s$), the tsunami wave force resulting from the evaluation formulae presented by Arimitsu et al. (2012) and Takabatake et al. (2013) coincided approximately with the empirical results.
 - In a non-steady state where dynamic pressure was intensely observed ($t < 10s$), the tsunami wave force resulting from the evaluation formula presented by Arimitsu et al. (2012) generally coincided with the empirical results.
 - The calculation formula presented by Takabatake et al. (2013) was applicable during a quasi-

steady-state, and in a non-steady state where dynamic pressure was intensely observed ($t < 10s$), a tsunami wave force was obtained, depending on the case, that significantly surpassed the empirical results.

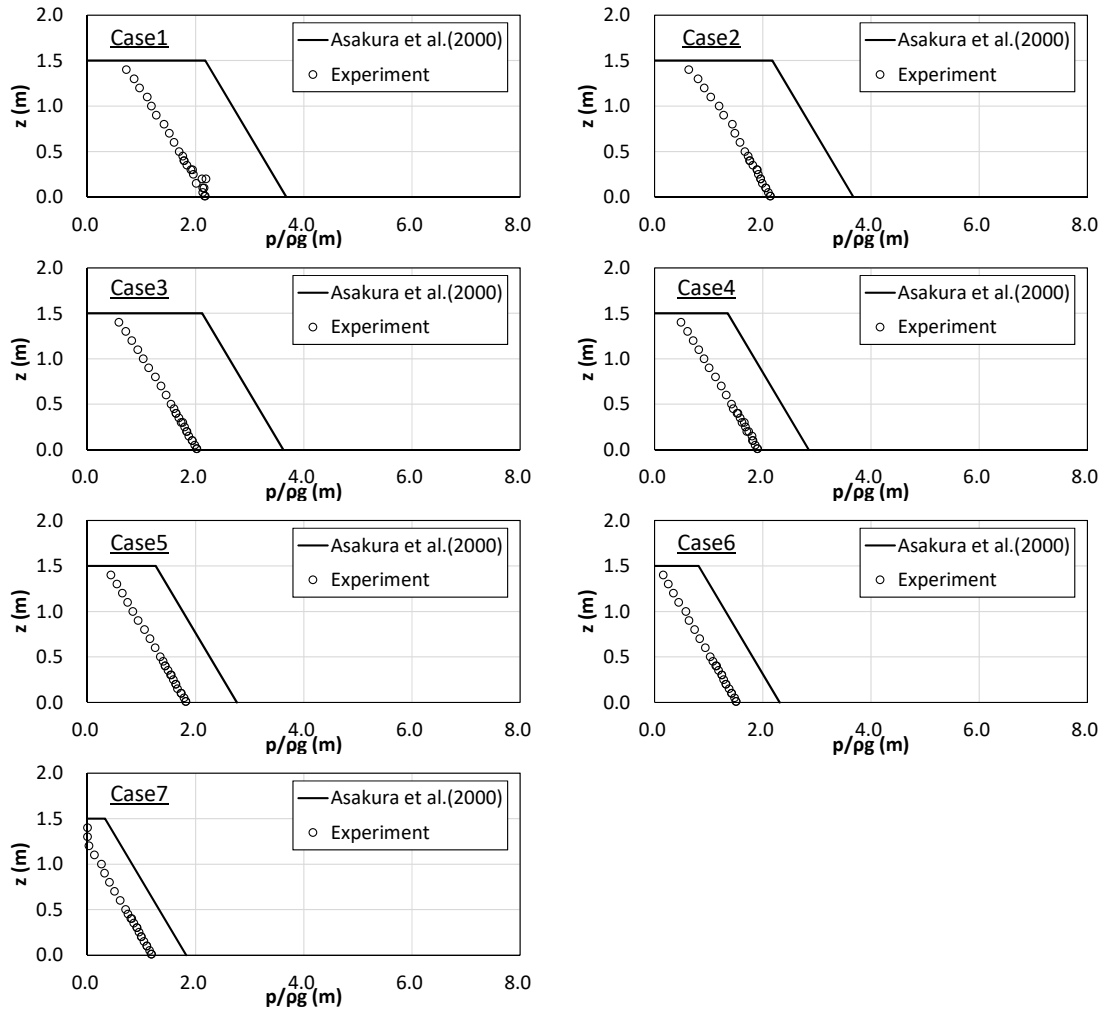


Figure 8.1.4-3 Comparison of maximum Tsunami wave pressure acting on the seawall

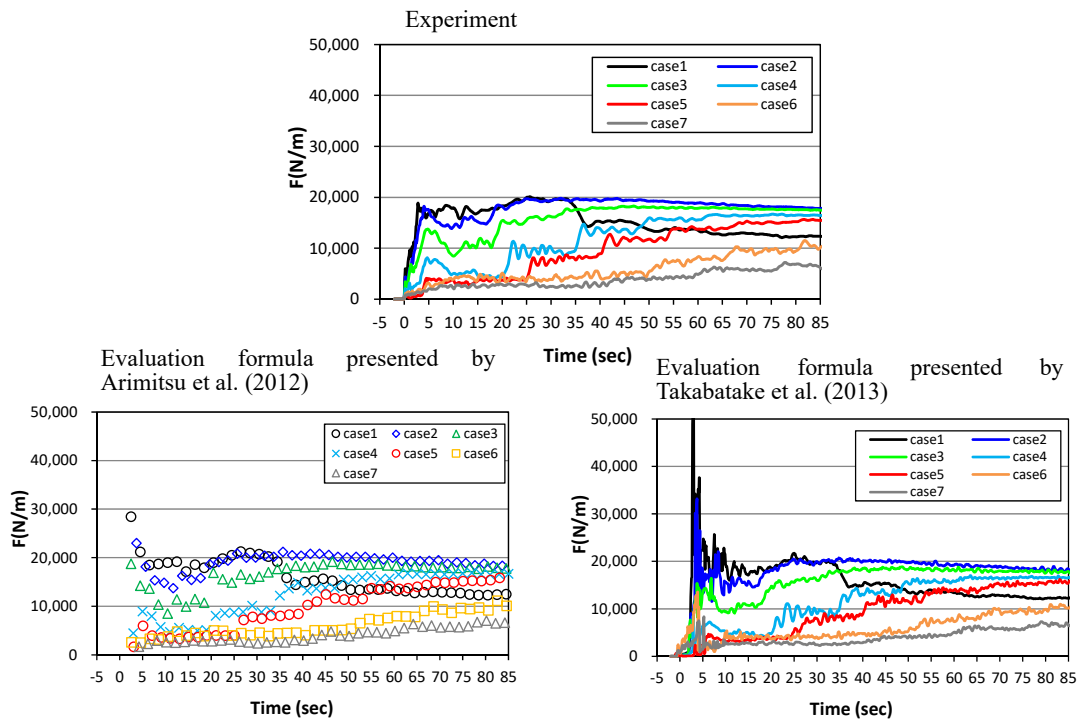


Figure 8.1.4-4 Empirical results of tsunami wave force time series acting on the seawall and results of calculations using tsunami wave force evaluation formulae

8.1.4.3. Tsunami wave force acting on cuboids (three-dimensional structures)

(1) Experiment overview

Figure 8.1.4-5 shows the experimental device for the test to assess tsunami wave force acting on cuboids (three-dimensional structures). For the experiment, a cuboid model was set up, which had a height of 2.0 m and width of 1.0m×1.0m, near the center of the water channel. The inclination of the cuboid model was varied, and measurements of the inundation depth, flow velocity, and pressure were taken during three types of flows having different inundation depths and flow velocities upstream of a seawall. Also, the inundation depth and flow velocity were measured for a case where a cuboid model was not set up (progressive wave).

Figures 8.1.4-6 to 8.1.4-9 show the empirical results of the time series tsunami shape for inundation depth, flow velocity, and other properties. Of the flow velocities measured at locations V1 and V2, consideration needs to be given to flow velocity during the periods of time indicated below, because a vertical mean flow velocity did not form for between 5 to 10 seconds after a reflected wave from the cuboid model and the movable weir at the downstream edge reached the measurement point.

Time periods when there is no vertical mean flow velocity

·Case where cuboid model is not set up

Type 1: $t = 18\text{s} \sim 24\text{s}$

Type 2: $t = 20\text{s} \sim 25\text{s}$

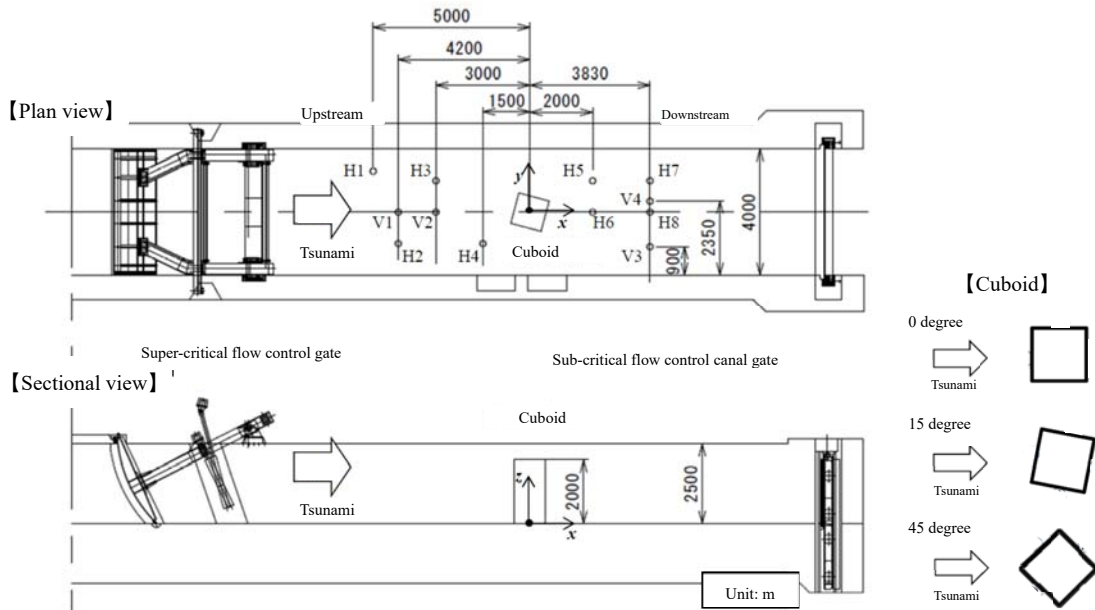
Type 3: $t = 23\text{s} \sim 30\text{s}$

·Case where cuboid model set up

Type 1: $t = 11\text{s} \sim 16\text{s}$

Type 2: $t = 15\text{s} \sim 20\text{s}$

Type 3: $t = 10\text{s} \sim 20\text{s}$



H1 - H8: Measuring points of inundation depth

V1: Measuring points of horizontal flow velocity by ADV

V2, V3, V4: Measuring point of horizontal flow velocity by aquadopp profiler

Pressure: Measurement is performed by installing pressure sensors of 6 points, 18points, 6 points respectively on the vertical line of the left end, the center, and the right end of the side face of the pressure gauge.

Figure 8.1.4-5 Experimental device for the test to assess tsunami wave force acting on cuboids (three-dimensional structures)

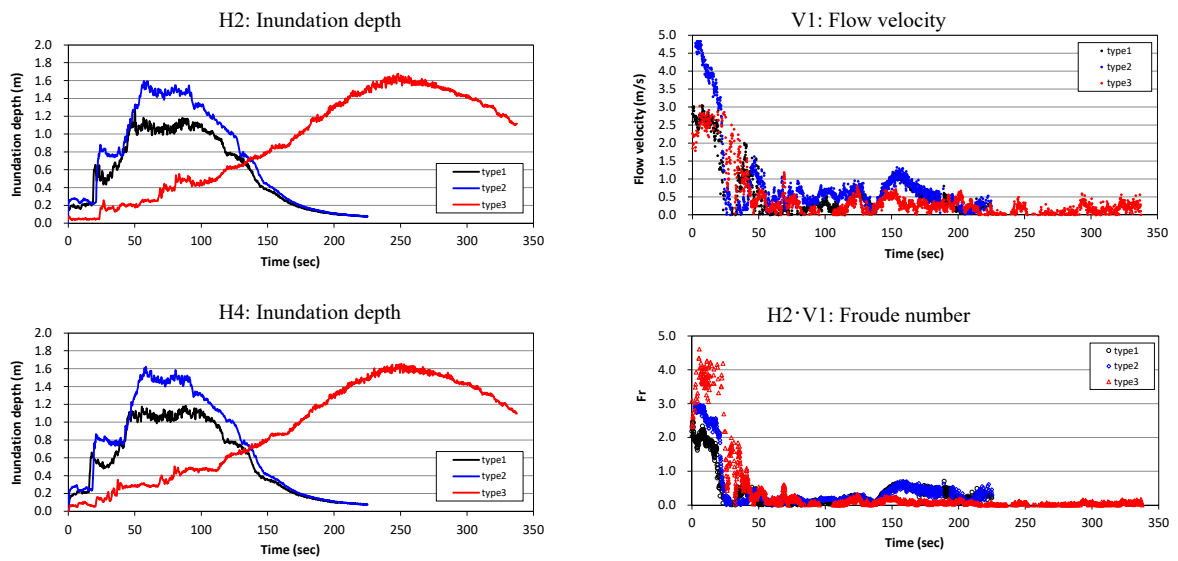


Figure 8.1.4-6 Time series of inundation depth in case without the cuboid model, flow velocity, Froude number (Flow type: type1~type3)

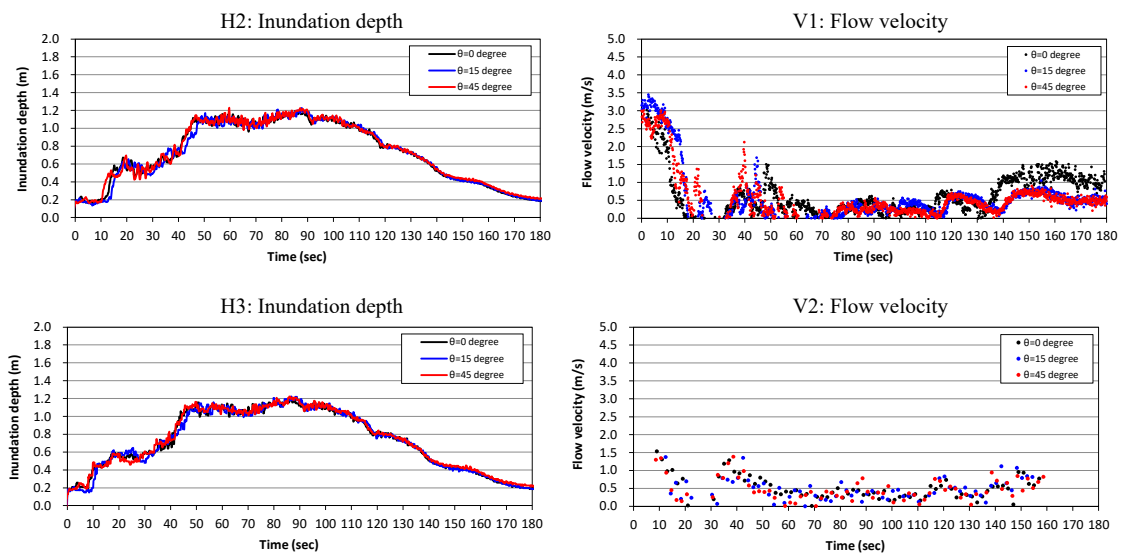


Figure 8.1.4-7 Time series of inundation depth and flow velocity in case with cuboid (Flow type: type1)

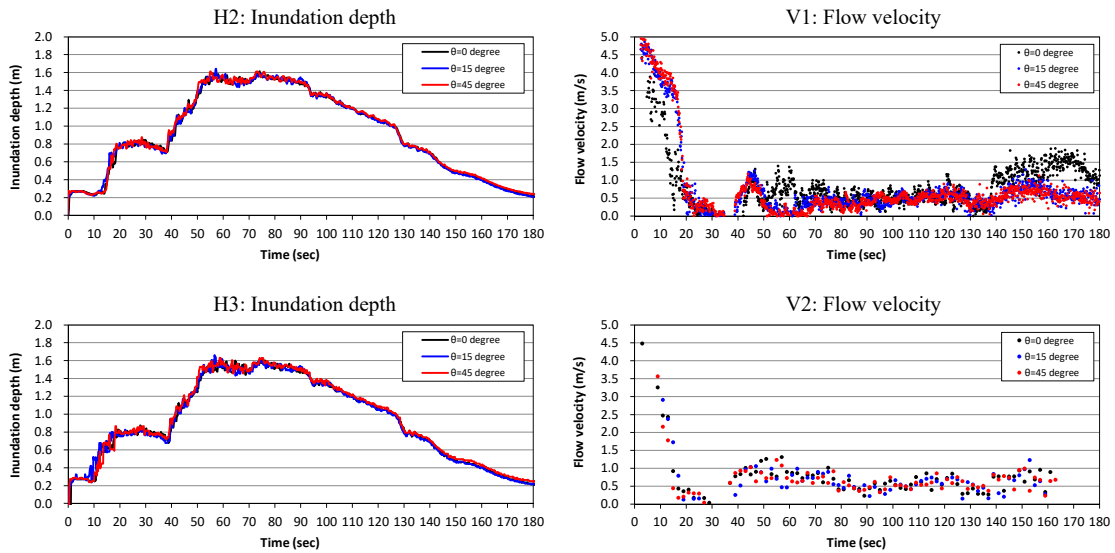


Figure 8.1.4-8 Time series of inundation depth and flow velocity in case with the cuboid model (Flow type: type2)

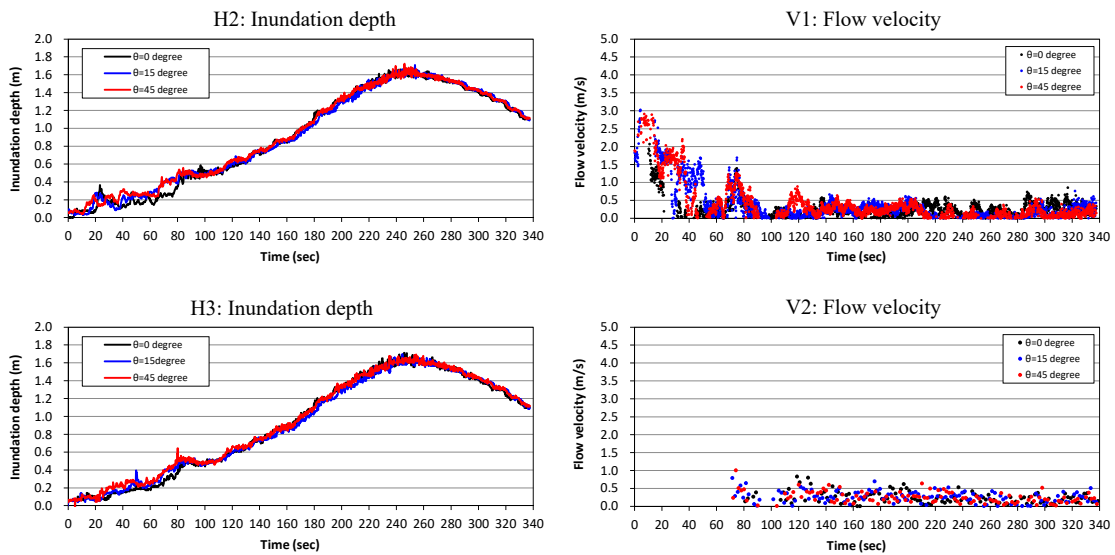


Figure 8.1.4-9 Time series of inundation depth and flow velocity in case with the cuboid model (Flow type: type3)

(2) Tsunami wave force calculation methods

Tsunami wave force evaluation formulae used in comparisons with empirical results are given below. The most appropriate positional data was selected from among the geodetic points for the empirical inundation depths and current velocities used in the calculation of tsunami wave force.

1) Tsunami wave force evaluation formula using hydraulic quantity in a state without structures

- Tsunami wave force evaluation formula presented by Asakura et al. (2000) (water depth coefficient $\alpha=3.0$)

The experiment measured the maximum inundation depth of the progressive wave, and the maximum inundation depth h_{imax} (type 1:1.18m, type 2: 1.62m, type 3: 1.65m) of the progressive wave at point H4 was used to calculate the tsunami wave force.

- Tsunami wave force evaluation formula presented by Asakura et al. (2002)

To calculate the tsunami wave force, the maximum inundation depth h_{imax} and flow velocity (time when h_{imax} occurs) of the progressive wave at points H2 and V1, which are shown in Table 8.1.4-1, were used.

- Tsunami wave force evaluation formula presented by Sakakiyama (2012)

To calculate the tsunami wave force, the maximum inundation depth h_{imax} and flow velocity (time when h_{imax} occurs) of the progressive wave at points H2 and V1, which are shown in Table 8.1.4-1, were used.

Table 8.1.4-1 Hydraulic quantity and water depth coefficient of progressive wave at point H2 and V1

Flow type	h_{imax} (m)	u_h (m/s)	F_r	α (Asakura et al., 2002)	α (Sakakiyama, 2012)
type1	1.28	0.56	0.16	1.19	1.22
type2	1.60	0.26	0.07	1.08	1.09
type3	1.68	0.18	0.04	1.05	1.06

2) Tsunami wave force evaluation formula using hydraulic quantity in a state with structures

- Tsunami wave force evaluation formula presented by Arimitsu et al. (2012)

To calculate the tsunami wave force, the time series tsunami shapes of inundation depth and flow velocity at points H3 and V2 were used.

- Tsunami wave force evaluation formula presented by Kihara et al. (2012)

To calculate the tsunami wave force, the time series tsunami shapes of inundation depth and flow velocity at points H2 and V1 were used.

The flow velocity in the empirical results was the flow velocity in a horizontal direction

(direction x as shown in Figure 8.1.4-5), so the flow velocity was corrected in accordance with the inclination of the cuboid and used in the tsunami wave force evaluation formulae presented by Arimitsu et al. (2012) and Kihara et al. (2012).

(3) Tsunami wave force calculation results

1) Tsunami wave force evaluation formula using hydraulic quantity in a state without structures

Figure 8.1.4-10 shows the results of a comparison of the maximum tsunami wave pressures as measured by tsunami wave pressure meters in experiments and the maximum tsunami wave pressure according to the evaluation formulae. The maximum wave pressure in the empirical results is based on a zero degree inclination of the cuboid and measurement aspect [1] where the maximum tsunami wave force is obtained.

The features are shown below for each tsunami wave force evaluation formula, which have been obtained from the results of comparisons of these formulae.

- The maximum tsunami wave pressure according to the evaluation formula presented by Asakura et al. (2000) was approximately 3 times the empirical results, obtaining results that sufficiently encompass the empirical results.
- The maximum tsunami wave pressure resulting from the evaluation formulae presented by Asakura et al. (2002) and Sakakiyama (2012) generally coincide with the empirical results.

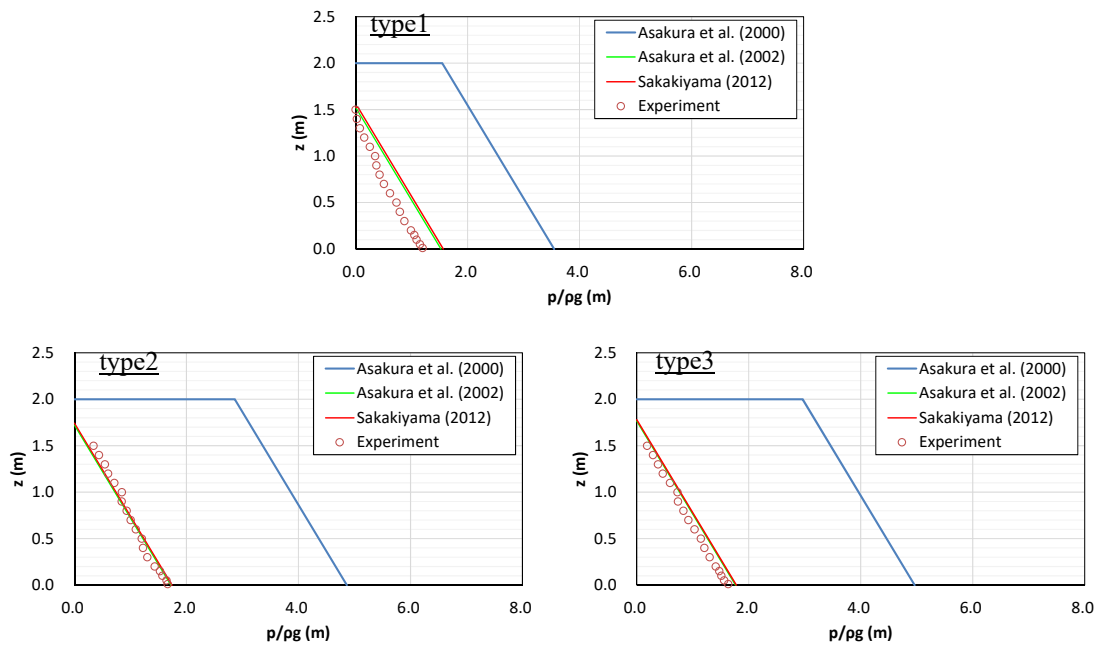


Figure 8.1.4-10 Comparison of maximum tsunami wave pressure acting on the cuboid model

2) Tsunami wave force evaluation formulae using hydraulic quantity in a state with structures

Table 8.1.4-2 shows the maximum tsunami wave force based on tsunami wave force

evaluation formulae and empirical results. Taking into account the Froude number time series tsunami shapes where models were not set up and the time periods when there is no flow velocity, $t < 10s$ is regarded as a non-steady state and $t \geq 10s$ a quasi-steady state, and the maximum tsunami wave forces were consolidated according to each state. Also, Figure 8.1.4-11 uses the example of a zero degree inclining cuboid to show the empirical results according to a time series tsunami wave force acting on the cuboid and the results calculated using tsunami wave force evaluation formula.

The features are shown below of each tsunami wave force evaluation formula, which have been obtained from the results of comparisons of these formulae.

- In a quasi-steady state ($t \geq 10s$), the tsunami wave force evaluation formulae presented by Kihara et al. (2012) and Arimitsu et al. (2012) coincided approximately with the empirical results.
- In a non-steady state ($t < 10s$), the tsunami wave force resulting from the evaluation formula presented by Arimitsu et al. (2012) generally coincided with maximum tsunami wave force in the experiments.
- The calculation formula presented by Kihara et al. (2012) was applicable during a quasi-steady state, and in a non-steady state, a tsunami wave force was obtained depending on the case that significantly surpassed the empirical results.

Table 8.1.4-2 Comparison of maximum tsunami wave force acting on the cuboid model

Unit: kN/m

Flow type	Cuboid angle (degree)	Maximum Tsunami wave force					
		Experiment		Arimitsu et al. (2012)		Kihara et al. (2012)	
		In a non-steady state ($t < 10s$)	In a quasi-steady state ($t \geq 10s$)	In a non-steady state ($t < 10s$)	In a quasi-steady state ($t \geq 10s$)	In a non-steady state ($t < 10s$)	In a quasi-steady state ($t \geq 10s$)
type1	0	1.6	7.4	1.2	7.1	2.9	8.0
	15	1.8	7.4	-	7.3	4.3	7.9
	45	1.3	7.4	0.9	7.5	1.3	7.4
type2	0	6.4	14.2	6.3	14.6	7.9	14.4
	15	6.0	14.5	-	13.6	9.5	13.3
	45	4.2	12.7	1.8	13.4	4.0	12.8
type3	0	0.7	13.2	-	13.4	-	13.9
	15	0.4	13.3	-	13.1	-	14.4
	45	0.2	13.3	-	13.5	-	14.6

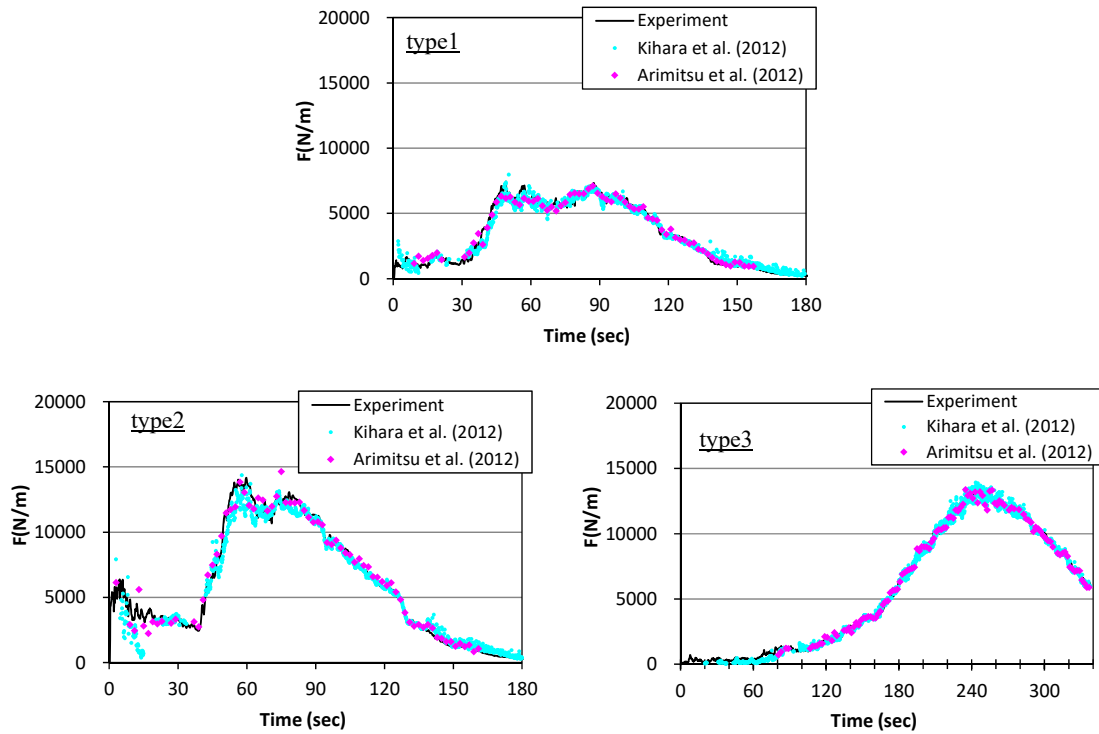


Figure 8.1.4-11 Comparison of time series of tsunami wave force acting on the cuboid model (Cuboid angle: 0 degree)

8.1.4.4. Tsunami wave force calculations using calculation results from plane two-dimensional models

(1) Examination overview

Focusing on tests for assessing tsunami wave force acting on cuboids (three-dimensional structures), the tsunami wave force acting on the structure was calculated by finding the inundation depth and flow velocity at appropriate positions corresponding to tsunami wave force evaluation formulae based upon numerical simulations using plane two-dimensional models that focused on a non-steady state immediately after a tsunami arrives in front of a structure.

(2) Simulating conditions

Of the tests for assessing tsunami wave force acting on cuboids, the target experiments were cases where a cuboid model was set up at an inclination of zero degrees in a type 1 flow. Figure 8.1.4-12 shows the numerical experiment water route used for the numerical simulations with a plane two-dimensional model. Also, Table 8.1.4-3 shows the principle simulating conditions.

For the numerical simulations of tsunami, a method was used that differentiated the continuity equation and nonlinear long-wave theory equation by means of a staggered leapfrog method. So that the conditions would be the same as the experiments, a storage portion and gate

were simulated at the upstream boundary and the pass-through flow rate is given according to Kuriki et al. (1996), and then, a movable weir was simulated at the downstream boundary and the overflow rate was taken into consideration according to Honma et al. (1940) according to the time variation for the crest height. With respect to the upstream boundary, the storage water level in the storage portion was set at 4.0 m and the height of the gate opening at 0.1 m, because the flow rate per unit width was considered as a value that successfully reproduces the empirical results, based upon Kuriki et al. (1996), of the linear flow rate obtained from the inundation depth and flow velocity at points H2 and V1.

(3) Calculation results

As for the calculation results using a plane two-dimensional model, Figure 8.1.4-13 shows the time series tsunami shape for inundation depth and flow velocity. The features are given below for the inundation depth and flow velocity in front of the model and at points H2 and V1.

- For the inundation depth at point H2, the empirical results and calculation results coincide approximately, and the continuously high flow velocity, which was observed in the empirical results, was able to be reproduced for the flow velocity at point V1.
- The inundation depth in front of the model was shown to be twice that of the progressive wave at point H2, depending upon the effect of the wave reflected from the model.
- The flow velocity in front of the model was shown to be a maximum of about 3 m/s instantaneously when the tsunami arrived, but subsequently, the progressive wave and reflected wave overlapped, so the flow velocity became conspicuously lower.

(4) Tsunami wave force calculations using calculation results based upon plane two-dimensional models

The calculation results from the plane two-dimensional model (inundation depth and flow velocity) were used to calculate tsunami wave force. To calculate tsunami wave force, the tsunami wave force evaluation formula presented by Arimitsu et al. (2012) was utilized. Figures 8.1.4-14 and 8.1.4-15 show the empirical results of a tsunami wave force time series and tsunami wave pressure time series acting on a cuboid as well as the results calculated using the tsunami wave force evaluation formula. The empirical results were calculated using the results for measurement aspect 1, and the calculation results using the evaluation formula presented by Arimitsu et al. (2012) utilize the hydraulic quantity in front of the model.

The features are given below for tsunami wave force and pressure as calculated using the evaluation formula presented by Arimitsu et al. (2012).

- In a non-steady state ($t < 10$ s), the maximum tsunami wave force according to the evaluation formula presented by Arimitsu et al. (2012) was 1.7kN/m and the maximum tsunami wave

force according to the experiments was 1.6kN/m, showing that these coincided approximately.

- The tsunami wave force according to the evaluation formula presented by Arimitsu et al. (2012) showed the maximum value when the tsunami arrived, and although there was a tendency for the tsunami wave force time series to somewhat exceed the empirical results, it was able to be reproduced for the most part.
- The tsunami wave pressure distribution according to the evaluation formula presented by Arimitsu et al. (2012) was not able to be reproduced up to a distribution having a local maximum somewhat upward from the bottom surface as seen in the empirical results of $t=2.0s$ due to the characteristics of the evaluation formula.

Although the calculation formula presented by Arimitsu et al. (2012) was presented based on, among other data, the results of numerical simulations for experiments using the dam-break method, it was verified that the calculation formula was able to be applied to the estimation of tsunami wave force in a non-steady-state for the tsunami head, even in experiments that reproduce tsunami on a scale close to an actual phenomenon.

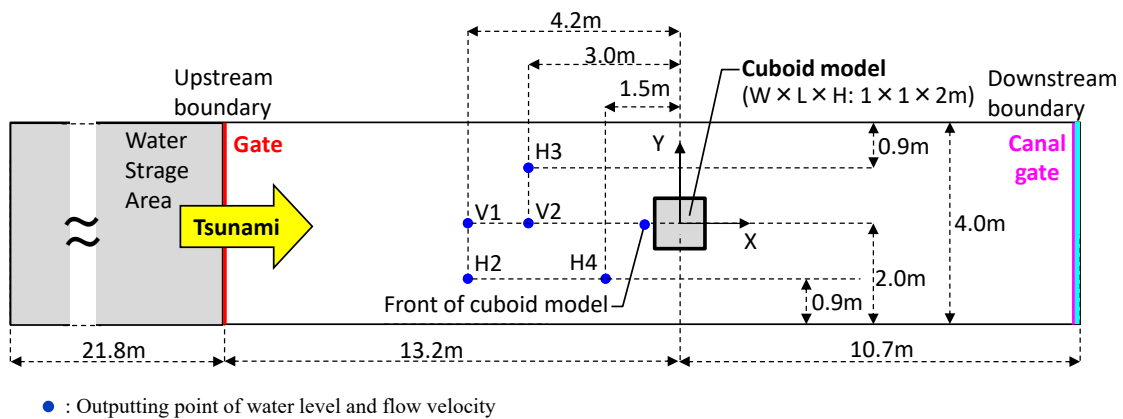


Figure 8.1.4-12 The numerical experiment water channel used for the numerical simulations with a plane two-dimensional model

Table 8.1.4-3 Simulating conditions used for the numerical simulations with a plane two-dimensional model

Item	Setting value
Government equations	Nonlinear long-wave theory equation and continuity equation
Upstream boundary	A storage portion and gate were simulated at the upstream boundary and the pass-through flow rate is given according to Kuriki et al. (1996)
Downstream boundary	A canal gate was simulated at the downstream boundary and the overflow rate was taken into consideration according to Honma et al. (1940) according to the time variation for the crest height
Grid sizes	0.05m
Computation time interval	0.001s
Simulating time	25s
Manning's coefficient of roughness	$n=0.010\text{m}^{-1/3}\cdot\text{s}$

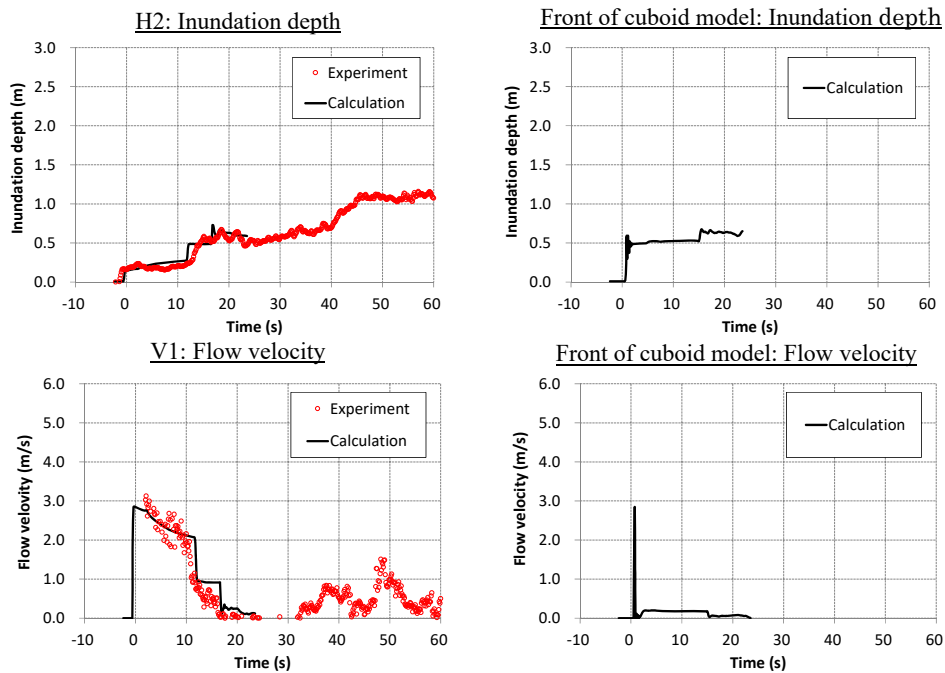


Figure 8.1.4-13 Time series of inundation depth and flow velocity

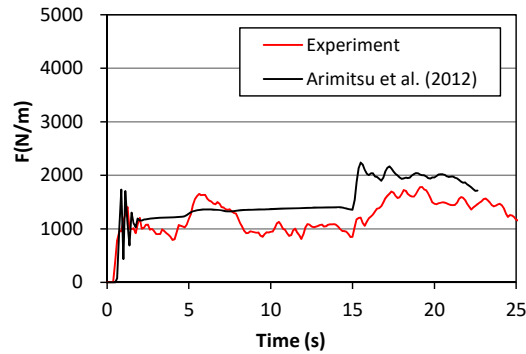


Figure 8.1.4-14 Time series of tsunami wave force acting on the cuboid model

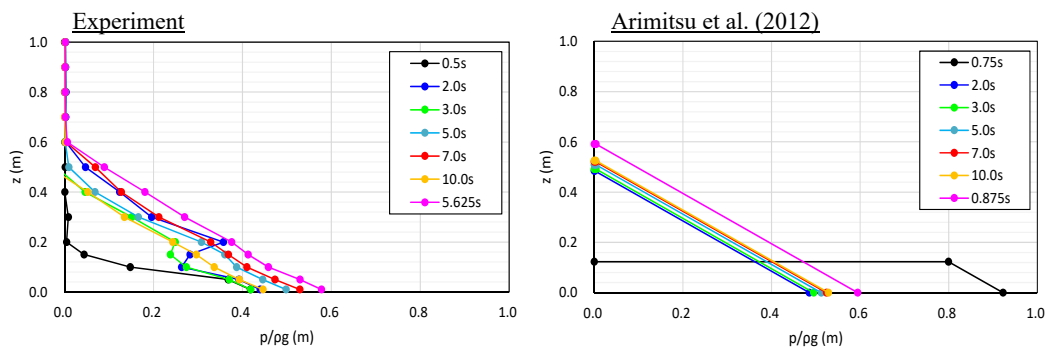


Figure 8.1.4-15 Time series of tsunami wave pressure acting on the cuboid model

8.2. Calculation of sediment transport

8.2.1. Examples of calculation methods

8.2.1.1. Model presented by Fujii et al. (1998)

(1) Friction velocity calculation formula

For calculation of friction velocity u_* , Kobayashi et al. (1996) used a logarithmic law shown in the following equation that may be applied under tsunami.

However, in the area of narrowing, the effect of the pressure gradient accompanying flow acceleration and deceleration makes the vertical distribution of current velocity uniform and the bottom shear stress increase, so Fujii et al. (1998) used a method for assessing bottom shear stress below the pressure gradient. u_* is calculated using an equation where the log-wake law for current velocity distribution is integrated in a vertical direction.

(2) Bed load equation

Kobayashi et al. (1996) used trap experiments to find an appropriate bed load transport

equation coefficient where the bed load volume is proportional to the Shields number τ raised to the power of 1.5. That was referenced when using the following equation for bed load transport volume.

$$Q = 80 \tau^{1.5} \sqrt{sgd^3}$$

where, Q : bed load transport rate per unit width per unit time, τ : Shields number, s : underwater density of sand, and g : acceleration of gravity.

(3) Consideration of suspended sediment

Models have been proposed that mix advection-diffusion and local flux, in which part of the total bed load transport rate behaves as a local flux governed primarily by external force at the location and the remainder behaves in accordance with the advection-diffusion equation for a single layer as a suspended component. Although this model is incapable of considering up to non-equilibrium relating to vertical distribution of the suspended sediment concentration, it is characterized by the capability to take into account non-equilibrium that emerges due to delay in the total bed load transport rate flux following sudden changes in the external force.

8.2.1.2. Model presented by Takahashi et al. (1999)

(1) Friction velocity calculation formula

An evaluation is made based upon friction force according to Manning's roughness coefficient used in a non-linear longwave equation.

(2) Bed load equation, pickup rate equation, and deposition rate equation

Bed load transport volume Q , suspended sediment pickup rate E , deposition rate S are expressed in the following formula.

$$Q = 21 \tau^{3/2} \sqrt{sgd^3}$$

$$E = 0.012 \tau^2 \sqrt{sgd} \cdot \sigma$$

$$S = w \bar{C} \cdot \sigma$$

where, τ : Shields number, S : underwater density of sand, g : acceleration of gravity, d : sand particle size, σ : sand density, w : sedimentation rate, and \bar{C} : mean suspended sediment concentration.

(3) Consideration of suspended sediment

For the calculation of sediment transport, an equation of sediment transport continuity and an equation for sand volume exchanged between the bed load layer and suspended sand layer will be used. Because this model does not assume an equilibrium state where pickup rate and

deposition rate are in balance, it may also be applied to suspended sediment conditions in non-equilibrium that occur due to non-steady dragging power.

8.2.1.3. Model presented by Ikeno et al. (2009)

The bed load equation differs from that of the model presented by Takahashi et al. (1999).

(1) Bed load equation: Ashida and Michiue (1972)

$$Q = 17 \sqrt{sgd}^3 \tau^{1.5} (1 - \tau_c / \tau) (1 - u_{*c} / u_*)$$

where, Q : Bed load transport volume per unit width per unit time, τ : Shields number, S : underwater density of sand, g : acceleration of gravity, d : sand particle size, τ_c : critical Shields number, and u_{*c} : critical friction velocity.

(2) Pickup rate equation

The calculation formula for dimensionless pickup rate is shown below.

$$\frac{E}{\sqrt{sgd}} = a P_1^{0.2} P_2^{1.6} (\tau - \tau_c)^2$$

$$P_1 = \nu / sgd^{\hat{p}}$$

$$P_2 = w / (sgd)^{0.5}$$

where, a : coefficient, ν : viscosity coefficient, and w : sedimentation rate.

When the sand particle size is 0.08mm and $a=0.15$, the pickup rate coefficient is 0.0056.

When the sand particle size is 0.2mm and $a=0.15$, the pickup rate coefficient is 0.015.

(3) Deposition rate equation

There are cases where the mean concentration and bottom concentration are used as the concentration in the bed load deposition rate equation.

8.2.1.4. Model presented by Takahashi et al. (2011)

With respect to the pickup rate equation and bed load equation presented by Takahashi et al. (1999), the hydraulic model experiments were conducted, and a model improved so that particle size dependence is taken into account.

Hydraulic model experiments were conducted using sand having three different particle sizes where the median diameters are 0.166mm, 0.394mm, and 0.267mm.

(1) Bed load equation

$$Q = 5.6\tau^{1.5}\sqrt{sgd^3} (d = 0.166\text{ mm})$$

$$Q = 4.0\tau^{1.5}\sqrt{sgd^3} (d = 0.267\text{ mm})$$

$$Q = 2.6\tau^{1.5}\sqrt{sgd^3} (d = 0.394\text{ mm})$$

(2) Pickup rate equation

$$E = 7.0 \times 10^{-5} \tau^2 \sqrt{sgd} \cdot \sigma (d = 0.166\text{ mm})$$

$$E = 4.4 \times 10^{-5} \tau^2 \sqrt{sgd} \cdot \sigma (d = 0.267\text{ mm})$$

$$E = 1.6 \times 10^{-5} \tau^2 \sqrt{sgd} \cdot \sigma (d = 0.394\text{ mm})$$

8.2.2. Calculation example: Hachinohe port

8.2.2.1. Examination overview

Calculations were performed to reproduce sediment transport at Hachinohe port with regard to the Chile tsunami on May 24, 1960. Two methods, one presented by Takahashi et al. (1999) and the other presented by Ikeno et al. (2009), were the methods used for calculation of sediment transport, and calculations of three cases were performed, in which the upper concentration limit for suspended sediment were set at 1%, 2% and 5%. For the coefficient presented by Ikeno et al. (2009), a was set at 0.15, and the volume concentration for the bottom was used when calculating the deposition rate.

8.2.2.2. Calculation region and modeling

The range analyzed in the numerical simulation was the region enclosed within the rectangle in Figure 8.2.2-1 (range extending approx. 3.2 km east to west, and approx. 2.2 km north to south). A diagram of the modeled water depths is given in Figure 8.2.2-2. Elevation data was input also for the grids on land (water depth of 0 m or greater) at the point in time during the calculation initial period, and run-up calculations performed. However, with respect to the grids on land at the point in time during the calculation initial period, the calculations were performed with a configuration where only deposits resulted but erosion did not when sediment transport was calculated.

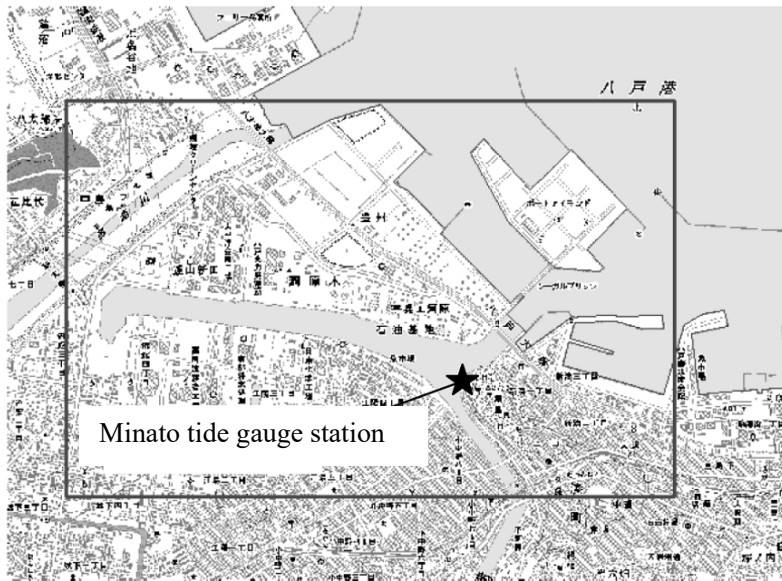


Figure 8.2.2-1 Analysis area

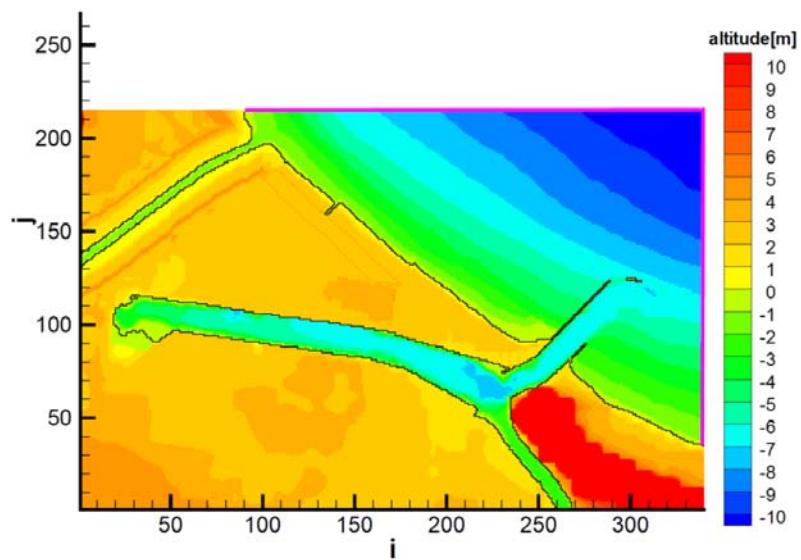


Figure 8.2.2-2 Analysis area (i, j are grid number.)

8.2.2.3 Calculation conditions

Table 8.2.2-1 shows calculation condition list of tsunami numerical simulation and calculating the sediment transport.

Table 8.2.2-1 Calculation conditions list

Parameter	Calculation conditions
Computational Region	Around Hachinohe Port (range extending approx. 3.2 km east to west, and approx. 2.2 km north to south)
Grid sizes	10.3m
Computation time interval	0.45 seconds
Fundamental equation of fluid	The Nonlinear Shallow Water Wave
Simulating time	10 hours
Land side boundary condition	Considering run up
Offshore side boundary condition	Input the waveform of the neighborhood of breakwater tip The tide level is T.P.±0.0m
Bottom friction	Roughness coefficient of Manning: $n=0.03\text{m}^{-1/3}\text{s}$
Horizontal eddy viscosity coefficient	$10\text{m}^2/\text{s}$
Particle size	0.26mm
Density of sand	$2,675\text{kg}/\text{m}^3$
Porosity	0.4
Sedimentation rate	$0.035\text{m}/\text{s}$ (Rubey, 1933)

8.2.2.4. Offing boundary conditions

For the offing boundary conditions pertaining to tsunami height, the water level in Figure 8.2.2-4 is given within the range indicated by the arrow in Figure 8.2.2-3. In order to verify the reproducibility of tsunami height calculations, a comparison was conducted of the time waveforms in tidal observation records (Japan Meteorological Agency) and calculated results at Minato tide gauge stations (Figure 8.2.2-5).

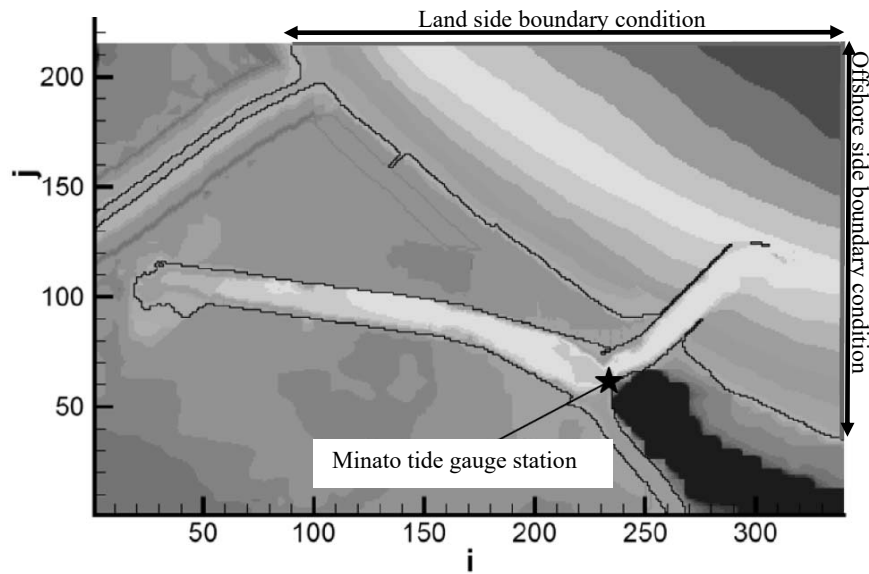


Figure 8.2.2-3 The offshore side boundary where the time waveform was input (i, j are grid number)

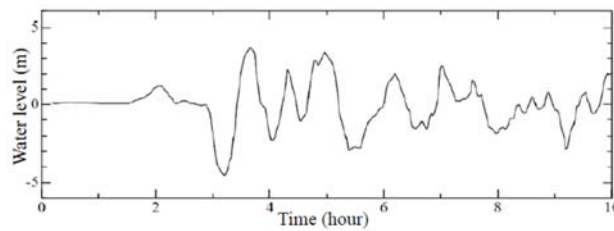


Figure 8.2.2-4 Time waveform of incident tsunami

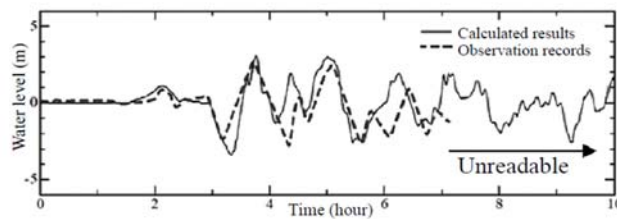


Figure 8.2.2-5 Comparison of calculation results and tide gauge records (Japan Meteorological Agency)

8.2.2.5. Observed values

In order to verify the distribution map for variation in the sea bottom topography change with numerical simulations, observation data (Figure 8.2.2-8) of variation in the sea bottom topography change using depth maps before and after the tsunami strike (Figure 8.2.2-6 and 8.2.2-7) was prepared.

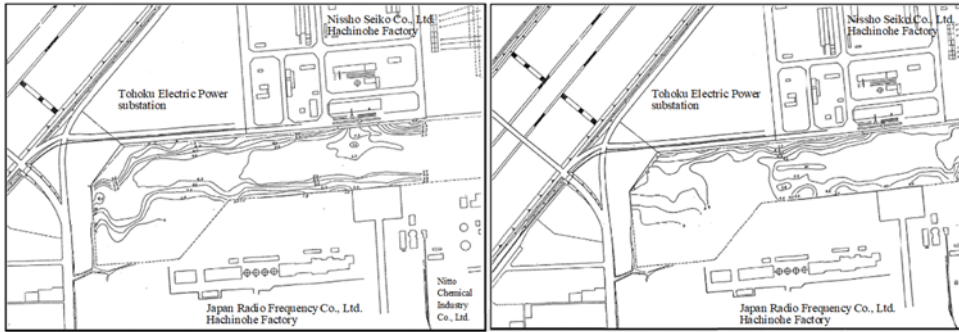


Figure 8.2.2-6 Bathymetry before and after the Chilean Tsunami's strike -back of port- (Left: April 1960, Right: June 1960)

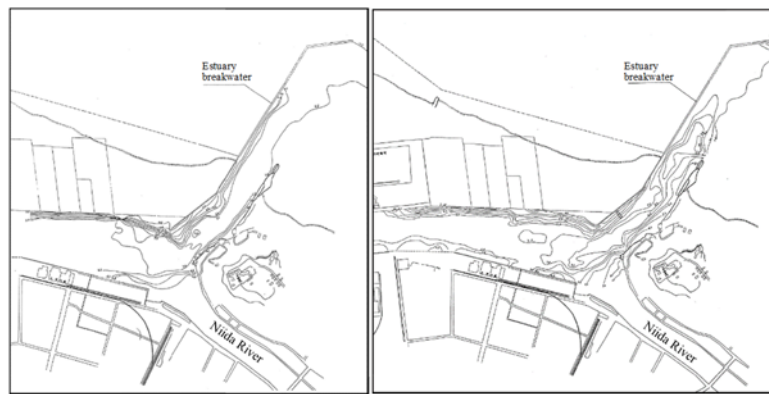


Figure 8.2.2-7 Bathymetry before and after the Chilean Tsunami's strike -mouth of port- (Left: April 1960, Right: June 1960)

Source: Ministry of Transport (1961)

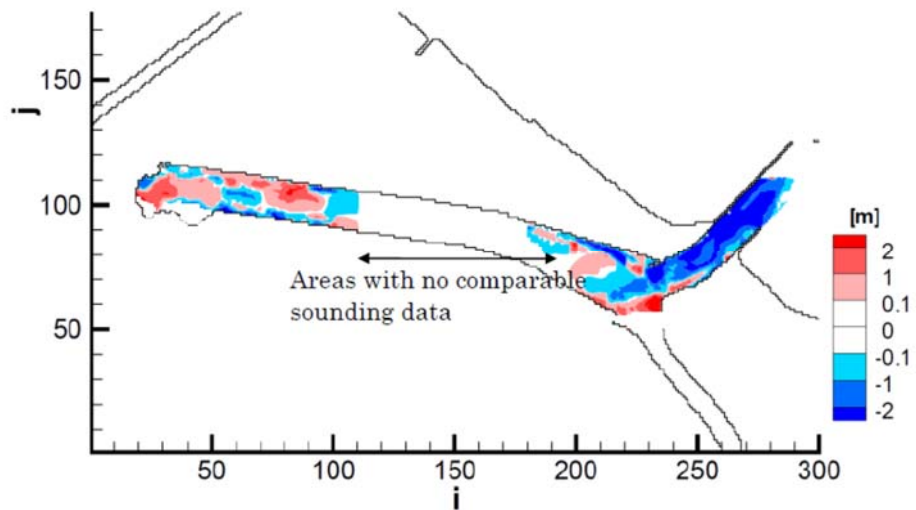


Figure 8.2.2-8 Topography changes created from sounded data (i, j are grid number)

8.2.2.6. Examination results

(1) Qualitative evaluation using distribution map

Figures 8.2.2-9 to 8.2.2-14 show distribution maps of the final extent of topography change.

There are six calculation cases:

Takahashi et al. (1999)

upper concentrations of suspended sediment: 1%, 2%, and 5%

Ikeno et al. (2009)

upper concentrations of suspended sediment: 1%, 2%, and 5%

As presented by Ikeno et al. (2009) a is 0.15 ($Y=aX^2$).

From a comparison of the observed values and a map showing the distribution of the final topography change, it may be said that the trends in sea bottom topography change were able to be reproduced well through measurements of erosion at the harbor entrance, small deposits at branch points, and deposits at the innermost part of the harbor. Little differences were found between Takahashi et al. (1999) and Ikeno et al. (2009), and both models provided good reproductions of the extent of sea bottom topography change where the upper concentration limit for suspended sediment were between 1% and 2% and found that 5% was an overestimate.

With respect to Ikeno et al. (2009), the maximum values for topography change where the upper concentration limit for suspended sediment was 2%, which the reproducibility was good, were found near the harbor entrance, and the maximum value for sediment was 8.4 m and the maximum value for erosion was 6.5 m (Figure 8.2.2-15).

* i,j are grid number

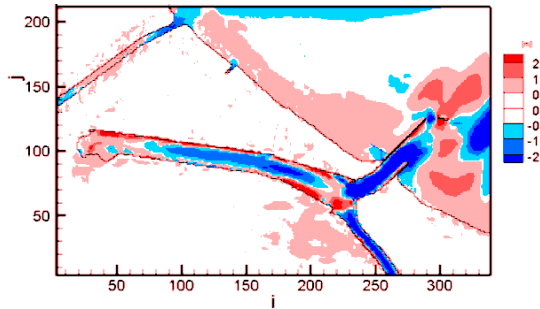


Figure 8.2.2-9 Distribution maps of the final extent of topography change Takahashi et al. (1999)

Upper concentration limit for suspended sediment 1%

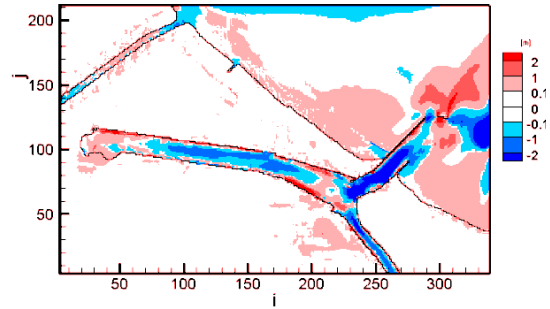


Figure 8.2.2-12 Distribution maps of the final extent of topography change Ikeno et al. (2009)

$a=0.15(Y=aX^2)$ Upper concentration limit for suspended sediment 1%

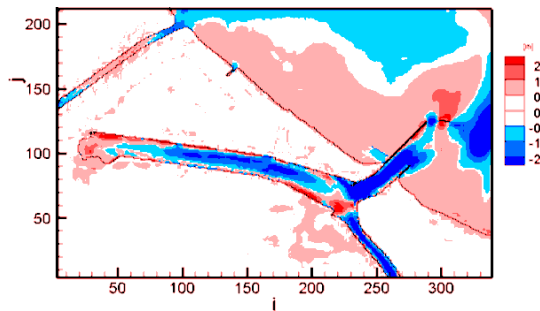


Figure 8.2.2-10 Distribution maps of the final extent of topography change Takahashi et al. (1999)

Upper concentration limit for suspended sediment 2%

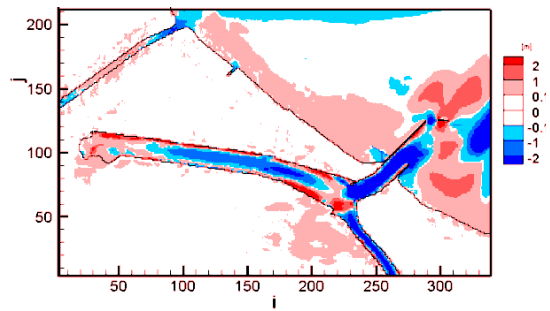


Figure 8.2.2-13 Distribution maps of the final extent of topography change Ikeno et al. (2009)

$a=0.15(Y=aX^2)$ Upper concentration limit for suspended sediment 2%

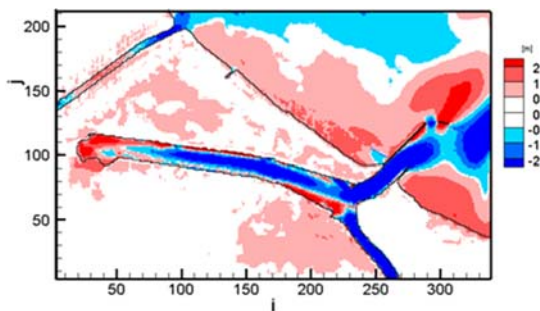


Figure 8.2.2-11 Distribution maps of the final extent of topography change Takahashi et al. (1999)

Upper concentration limit for suspended sediment 5%

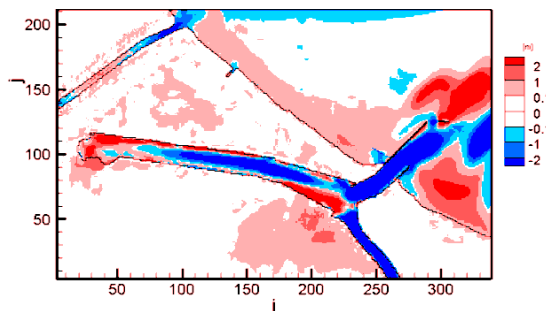


Figure 8.2.2-14 Distribution maps of the final extent of topography change Ikeno et al. (2009)

$a=0.15(Y=aX^2)$ Upper concentration limit for suspended sediment 5%

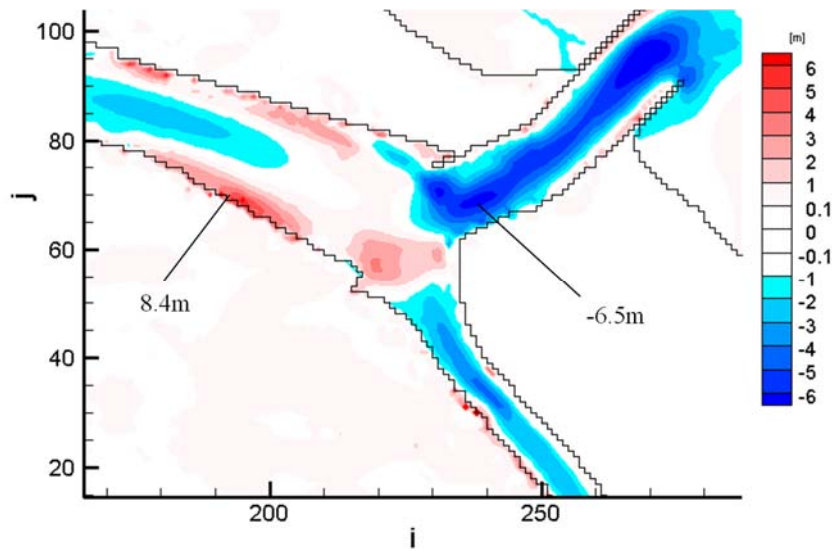


Figure 8.2.2-15 The maximum amount of sediment, erosion (Ikano et al. 2009)
 $a=0.15(Y=aX^2)$ Upper concentration limit for suspended sediment 2%
 * i, j are grid number

(2) Quantitative evaluation of sediment and erosion volume

The harbor interior was partitioned into four regions (Figure 8.2.2-16), and the sediment volume and erosion volume were calculated for each region. In the region enclosed within the rectangle in Figure 8.2.2-16, the sediment volume and erosion volume were calculated only for the grids set in the sea area during the calculation initial period.

Of the four regions, the results of a comparison with observation data for the regions other than part 3 showed that reproducibility was good for the upper concentration limit for suspended sediment from 1% to 2% for both Takahashi et al. (1999) and Ikano et al. (2009), and it was found that 5% would result in an overestimation (Figures 8.2.2-17 to 8.2.2-20, Table 8.2.2-2, and Table 8.2.2-3).

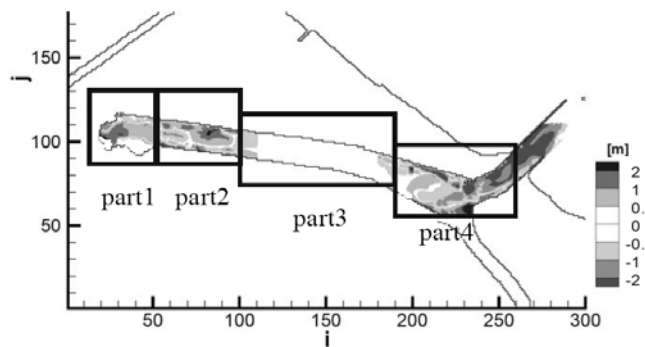


Figure 8.2.2-16 Division of the domain that calculated amount of sediment, erosion

1) Takahashi et al. (1999)

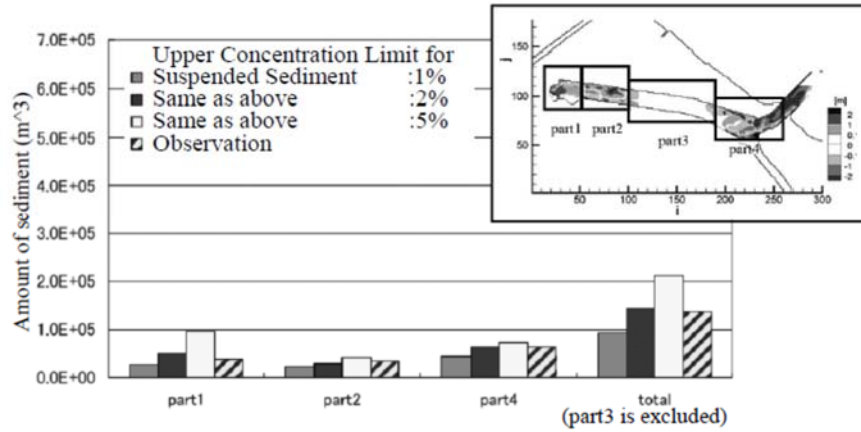


Figure 8.2.2-17 Amount of sediment per domain (Takahashi et al., 1999)

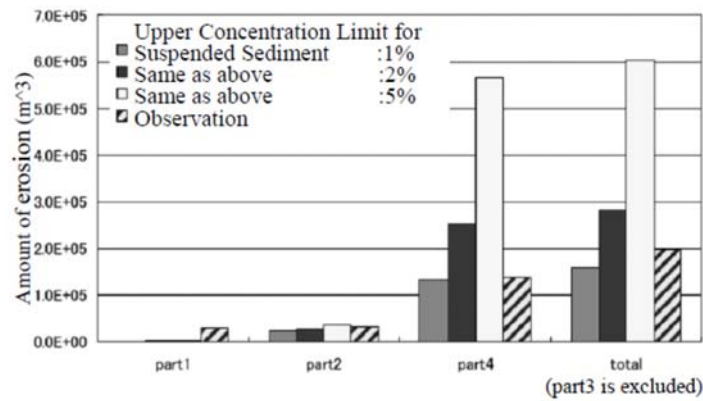


Figure 8.2.2-18 Amount of erosion per domain (Takahashi et al., 1999)

Table 8.2.2-2 Amount of sediment and erosion per domain (Takahashi et al., 1999)

domain	Upper concentration limit for suspended sediment						Observation	
	1%		2%		5%		Observation	
	Sediment (m³)	Erosion (m³)	Sediment (m³)	Erosion (m³)	Sediment (m³)	Erosion (m³)	Sediment (m³)	Erosion (m³)
part1	2.7E+04	1.4E+03	5.0E+04	1.7E+03	9.5E+04	1.5E+03	3.9E+04	2.9E+04
part2	2.2E+04	2.4E+04	3.0E+04	2.9E+04	4.2E+04	3.5E+04	3.5E+04	3.2E+04
part3	3.8E+04	8.6E+04	4.2E+04	1.7E+05	4.8E+04	2.4E+05	-	-
part4	4.3E+04	1.3E+05	6.4E+04	2.5E+05	7.2E+04	5.7E+05	6.4E+04	1.4E+05
Total	1.3E+05	2.5E+05	1.8E+05	4.5E+05	2.6E+05	8.4E+05	-	-
total (part3 is excluded)	9.2E+04	1.6E+05	1.4E+05	2.8E+05	2.1E+05	6.0E+05	1.4E+05	2.0E+5

2) Ikeno et al. (2009)

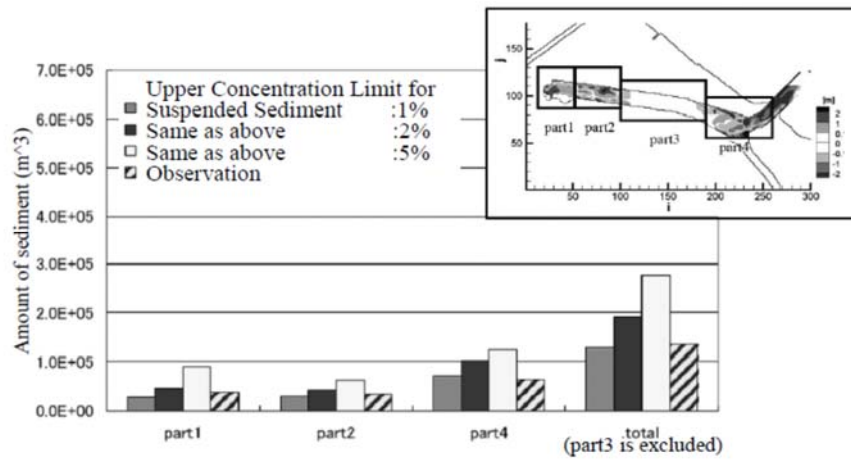


Figure 8.2.2-19 Amount of sediment per domain (Ikeno et al., 2009)

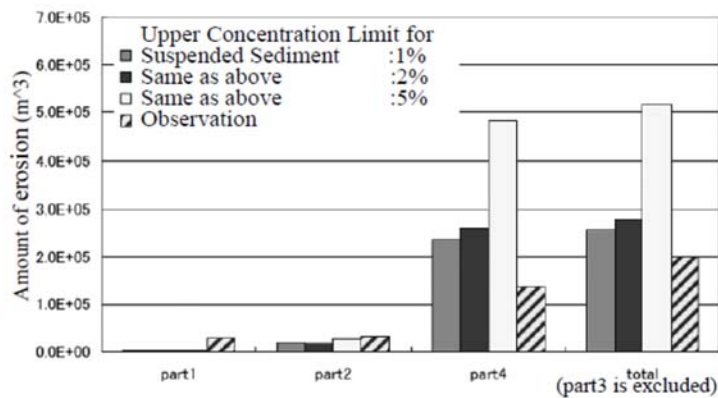


Figure 8.2.2-20 Amount of erosion per domain (Ikeno et al., 2009)

Table 8.2.2-3 Amount of sediment and erosion per domain (Ikeno et al., 2009)

domain	upper concentration limit for suspended sediment						Observation	
	1%		2%		5%		Sediment (m ³)	Erosion (m ³)
	Sediment (m ³)	Erosion (m ³)	Sediment (m ³)	Erosion (m ³)	Sediment (m ³)	Erosion (m ³)		
part1	2.7E+04	1.8E+03	4.5E+04	2.4E+03	8.9E+04	2.3E+03	3.9E+04	2.9E+04
part2	2.9E+04	1.9E+04	4.3E+04	1.7E+04	6.3E+04	2.6E+04	3.5E+04	3.2E+04
part3	5.1E+04	1.0E+05	6.8E+04	1.3E+05	6.8E+04	2.3E+05	-	-
part4	7.2E+04	2.4E+05	1.0E+05	2.6E+05	1.2E+05	4.9E+05	6.4E+04	1.4E+05
Total	1.8E+05	3.6E+05	2.6E+05	4.1E+05	3.4E+05	7.5E+05	-	-
total (part3 is excluded)	1.3E+04	2.6E+05	1.9E+05	2.8E+05	2.8E+05	5.2E+05	1.4E+05	2.0E+5

8.2.2.7. Friction velocity and Shields number

The friction velocity and Shields number are given below for a case of Ikeno et al. (2009) where the upper concentration limit for suspended sediment is 2% and $\alpha=0.15$.

u_* spatial mean maximum value: 13.7

Routh number (u_* / w_s): 3.9

where, w_s : sedimentation rate (particle size: 0.26mm, and calculated according to Rubey (1933)).

Spatial average of the Shields number: 1.14

Spatial average maximum value of the Shields number: 7.84

8.2.2.8. Summary

- Calculations were performed to reproduce topography change at Hachinohe port during the 1960 Chile tsunami.
- The simulation focused on Takahashi et al. (1999) and Ikeno et al. (2009), and both models were able to reproduce trends where occurred at the harbor entrance and sedimentation was deposited at the innermost part of the harbor. There were little differences between the two models.
- Both models provide a good reproducibility of a case where the upper concentration limit for suspended sediment was between 1% and 2%, and 5% resulted in an overestimate.

8.2.3. Examples and previous research on damage related to sediment transport

8.2.3.1. Examples of scouring phenomena during the 2011 Tohoku tsunami

Case studies from the following material were consolidated of damage from scouring and other phenomena around buildings and structures along the coastline due to sediment transport that occurred during the 2011 Tohoku tsunami.

- Port and Airport Research Institute, National Institute for Land and Infrastructure Management, and Fisheries Research Agency, “Report of Investigation of Earthquake and Tsunami Damage to Ports, Harbors, Airports and Fishing Ports Due to the Great East Japan Earthquake”, Technical Lectures on Ports, Harbors, Airports and Fishing Ports, May 2011.
- 2011 Great East Japan Earthquake Tsunami Joint Survey Group Report Meeting, July 2011.
- Great East Japan Earthquake Report Meeting, 2.4 Sea Coast, Characteristics of Damage to Coastal Structures and Hinterland from Tsunami (National Institute for Land and Infrastructure Management, Ministry of Land, Infrastructure, Transport and Tourism), April 2011

<http://www.nilim.go.jp/lab/bbg/saigai/h23tohoku/>

- 2011 Report on Investigation of Great East Japan Earthquake Damage (Building Research Institute)

<http://www.kenken.go.jp/japanese/contents/topics/20110311/0311report.html>

- Disaster Prevention Working Group, Ports Subcommittee, Council for Transport Policy under the Ministry of Land, Infrastructure, Transport and Tourism, “Comprehensive Approach to Tsunami Countermeasures for Harbours and Ports (Interim Report)”, July 2011.
- Disaster Prevention Working Group, Ports Subcommittee, Council for Transport Policy under the Ministry of Land, Infrastructure, Transport and Tourism, “Approach to Tsunami Countermeasures for Harbours and Ports”, June 2012.

(1) Investigation results

1) Examples of damage

Tomita (2011) and Sugano (2011) reported cases of damage that included scouring along the coastline (Hachinohe port), damage to corners of sheet pile-type quays and damage to straight portions of sheet pile-type quays (Soma port), and damage to corners of gravity-type quays (Hitachi port section of Ibaraki port), and that the damage increased due to the overlapping of ground motion, liquefaction, damage to pavement and sheet piles, scouring, differential water pressure, and tsunami wave pressure.

Takahashi (2011) presented the example of Hachinohe port where it has been estimated that a 6m high tsunami struck. More specifically, Takahashi (2011) reported that the fast flow of the tsunami caused about 10m of scouring on corners of wharves and at the breakwater opening. Also, the overturning of a caisson, which formed the corner of reclaimed land, was reported to be due to scouring along the sea bottom in front of the caisson.

Sakakiyama et al. (2011) reported examples of scouring that occurred behind sea embankments.

Suwa (2011) verified that, with regard to coastal structures along the coasts of Miyagi Prefecture and Iwate Prefecture, the significant overflow of embankments was also due to a damage to the embankments as well as topography change behind the embankments, and the overflow reached several meters, but Suwa reported three cases of damage to embankments: complete destruction of the embankments, scouring of the back slope and partial rupture only of the damaged crest, and no damage to the main embankment unit.

Building Research Institute (2012) found many traces of large holes due to scouring as the strong current acted on corners of structures during tsunami action, and that the scouring caused buildings to collapse and tilt, and the tsunami produced intense scouring that exposed many footings and pile heads.

2) Failure mechanisms

The Ministry of Land, Infrastructure, Transport and Tourism (2011) and Ministry of Land, Infrastructure, Transport and Tourism (2012) compiled mechanisms of how breakwaters and seawalls failed as well as how future countermeasures should be approached. With regard to breakwater failure mechanisms, these reports used the example of breakwaters at the entrance of Kamaishi port, and pointed out that, among other events, the caissons slid due to the difference in water levels outside and inside the port, foundation mounds were scoured due to the strong flow created by the water level difference, and caissons subsided and slid down. With regard to seawalls, these reports stated that there were many examples where overflow during leading waves scoured back slopes and slope toes resulting in collapses.

(2) Summary

- Examples were observed where the faster flow caused by the tsunami produced relatively extensive scouring on the corners of wharves and at breakwater openings.
- Examples were observed where scouring in front of corners of reclaimed land resulted in caissons overturning.
- At breakwaters, scouring of foundation mounds, which resulted from the strong flow produced by differences in water levels, occurred along with caissons sliding due to water level differences as well as caissons subsiding and sliding down.
- At seawalls, many examples were observed where overflow during the leading wave caused scouring of back slopes and slope toes, resulting in collapse.
- At revetments and other similar structures, cases were also observed where the leading wave damaged weak parts of structures and the backwash increased the damage at such locations as well as other examples where damage was sustained due to the action of the external force from both leading waves and backwash. Seismic ground motion, liquefaction, tsunami wave pressure, and scouring overlapped, increasing the damage.

Around buildings, many traces have been observed where, during the tsunami action, strong currents acted on corners and the scouring resulted in large holes. Situations resulted in buildings collapsing and tilting into holes created by the scouring. In addition, intense scouring, caused by the tsunami, exposed many footings and pile heads.

8.2.3.2. Previous studies on scouring

(1) Evaluations of scouring around buildings due to tsunami

There is an empirical formula presented by Noguchi et al. (1997), which is shown below, that serves as a formula for assessing scouring around structures. Noguchi et al. (1997) defined

the various quantities related to scouring as shown in Figure 8.2.3-1, and the magnitude of the standing vortex and the scouring depth are almost equal, so the scouring depth has been estimated by finding the magnitude of the standing vortex.

$$R = g^{-1/4} q^{1/2} z_f^{1/4}$$

where, R : scouring depth (m), g : acceleration of gravity (m/s^2), q : flow rate of falling water ($m^3/m/s$), and z_f : height from water level in front of revetment to crest of revetment (m).

Of the proposals for reasonably assessing the damage to land structures resulting from tsunami, Yamamoto et al. (2011) conducted multiple hydraulic model experiments with hydraulic models in order to develop a practical numerical prediction model for scouring of the lower part of revetments due to return flow, and thereby increase the understanding of scouring mechanisms and Yamamoto et al. (2011) proposed a method for assessing the maximum scouring depth and its position. Yamamoto et al. (2011) stated that the distance up to the location of maximum scouring is able to be found if the calculated value for parabolic movement is corrected using the peak current velocity of the return flow, and that the maximum scouring depth may be calculated by using the cumulative value for the vertical direction compound of motion energy or impulse per unit width of the returning flow water mass up to the peak current velocity.

FEMA (2012) is shown in Table 8.2.3-1 as the relationship between inundation depth and scouring depth according to Dames and Moore (1980). In keeping with the distance from the coastline and bottom material, the scouring depth is expressed as a percentage of the inundation depth. For example, in a case where the bottom material is loose sand and the inundation depth is 10m at a distance of 90m or more from the coastline, the scouring depth is calculated to be 6m.

Arikawa et al. (2014) used hydraulic model experiments to examine the extent of scouring behind a vertical embankment when a tsunami overflows the embankment. Arikawa et al. (2014) showed that overflow depth and scouring depth are in a highly correlated proportional relationship, and may be quantitatively assessed by means of a similarity law commensurate with the sedimentation rate (Figure 8.2.3-2).

(2) Examinations using numerical analysis

Goto et al. (2013) used a particle method-type numerical wave tank that allowed for the simplified treatment of moving bed boundaries interlinked with flow fields as well as the tracking in a Lagrange manner of the movement of caissons, covered blocks and mound rubble so as to conduct numerical simulations of the process of failure due to overflowing and scouring of composite breakwaters. The water level outside the harbor was held constant and the water level inside the harbor varied to compare failure processes, and in the case where the water level inside

the harbor was the lowest, the tsunami wave force caused caissons to slip before scouring occurred. In cases where the water level inside the harbor was somewhat high, it was confirmed that breakwaters failed due to the increased size of scouring holes, and in cases where the water level inside the harbor was the lowest and the levees had been widened, caisson movement was effectively suppressed and failure did not result.

Nakamura et al. (2015) focused on coastal embankments damaged due to the tsunami resulting from the 2011 Tohoku tsunami, and utilized actual scale numerical analysis to examine mechanisms of scouring development and the effectiveness of measures to counter scouring. The model, which was used in this study for performing numerical simulations of three-dimensional fluid, structures, topography change, and ground coupling, was comprised of a main solver that took into account changes in topography to analyze fluid motion in all gas-liquid phases comprised of incompressible fluid including fluid inside the gaps of moving beds, as well as a module based upon the VOF method for tracking the air liquid surface, a module for calculating topography change due to bed load and suspended sediment transport and analyzing the distribution of suspended sediment concentrations, and other modules (Nakamura et al., 2013; Nakamura and Mizutani, 2014).

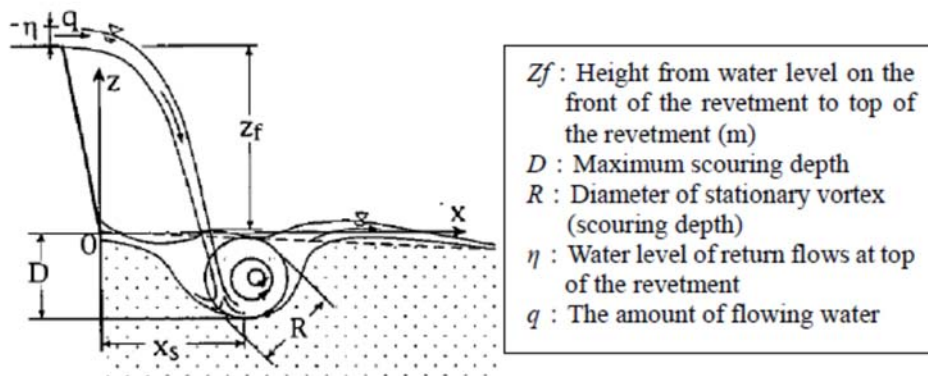


Figure 8.2.3-1 The various quantities related to scouring (Noguchi et al., 1997)

Table 8.2.3-1 Approximate scour depth as a percentage of inundation depth, d (Dames and Moore, 1980)

Soil type	Scour depth (% of d)	
	(Shoreline Distance < 300 feet)	(Shoreline Distance > 300 feet)
Loose sand	80	60
Dense sand	50	35
Soft silt	50	25
Stiff silt	25	15
Soft clay	25	15
Stiff clay	10	5

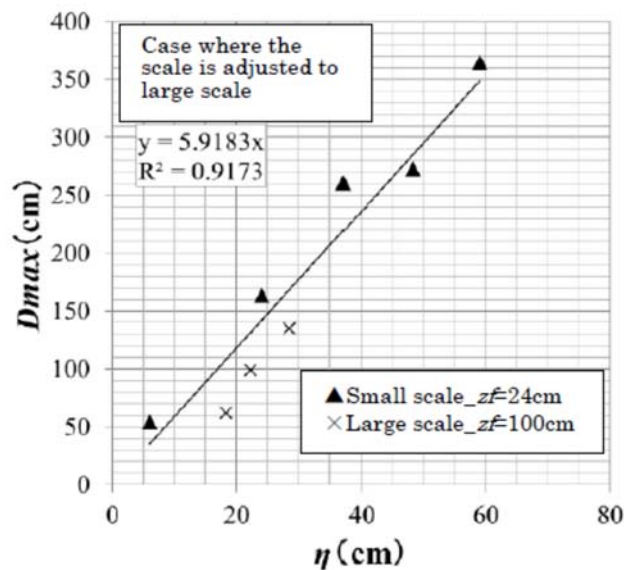


Figure 8.2.3-2 Relationship between overflow depth and scouring depth (Arikawa et al., 2014)

8.2.3.3. Previous studies on upper concentration limit for suspended sediment

When calculating bottom shear stress, the sediment transport calculation model presented by Takahashi et al. (1999) tends to overestimate bottom shear stress as total water depth is reduced. As bottom shear stress increases, lifting sand is supplied to the suspended sediment layer, and the concentration of suspended sediment increases. When calculating the pick-up rate and concentration of suspended sediment of these, it is ideal to use a model that takes into account physical mechanisms, but currently, methods that set an upper concentration limit for suspended sediment and restrain the overestimation of the volume of pick-up rate are often used.

With regard to the upper concentration limit for suspended sediment, there are cases where actual scale verification has been performed using actual measured values of the sea bottom topography change in harbors and ports during the Chile tsunami and the 2011 Tohoku tsunami in Tamada et al. (2009), Fujita et al. (2010), Kondo et al. (2012), Morishita et al. (2014) and other studies.

Tamada et al. (2009) calculated sediment transport in the sea bottom topography change of Kesenuma bay in Miyagi Prefecture at the time of the 1960 Chile tsunami, and conducted a parametric study of the calculation model grid size, particle size, and upper concentration limit for suspended sediment. With the exception of the maximum depth when the particle size was 0.001 mm, a trend was observed where the calculation results of cases where the upper concentration limit for suspended sediment was 5% showed a greater maximum depth and sediment deposit depth than the

results of calculations in a case where the concentration was 1%. Also, in a case where the particle size was 0.1 mm and the grid size 5 m, it was confirmed that there was a tendency to overestimate depth to be greater than the actual values when the upper concentration limit for suspended sediment was 5%. Based on these facts, it has been surmised that the upper concentration limit for suspended sediment in Kesennuma bay during the 1960 Chile earthquake tsunami was less than 5%.

Fujita et al. (2010) conducted an examination of sea bottom topography changes of Hachinohe port at the time of the 1960 Chile tsunami and conducted parametric studies of upper concentration limits for suspended sediment of 1%, 2%, and 5% using a particle size of 0.21 mm and a calculation model grid size of 10.3 m. The amount of topography change of each region (sediment volume and erosion volume) was tabulated and compared with the observed values, which showed that there was good reproducibility when the upper concentration limit for suspended sediment was set at 1% and 2%, and it was confirmed that an overestimate would result using a concentration limit of 5% (Figure 8.2.3-3).

Kondo et al. (2012) calculated sediment transport in the sea bottom topography change at Miyako port during the 2011 Tohoku tsunami. The examination was conducted using a particle size of 0.08 mm, an upper concentration limit for suspended sediment of 1%, and calculation model grid size of 10 m, and confirmed that the model presented by Takahashi et al. (1999) was able to reproduce with sufficient precision the actual topography change (Figure 8.2.3-4).

Morishita et al. (2014) calculated sediment transport in the sea bottom topography change of Kesennuma bay during the 2011 Tohoku tsunami, deduced four factors that predominantly contributed to sand movement (dimensionless dragging power, sediment transport equation coefficient, upper concentration limits for suspended sediment, and sedimentation rate), and modified the model. The upper concentration limit for suspended sediment should, intrinsically, be expressed as a function of the friction velocity, so the upper concentration limit for suspended sediment was set so that it varies according to current velocity. As for the factors other than upper concentration limit for suspended sediment, these were set along with modifying the sediment transport equation coefficient and dimensionless dragging power to significantly improve the distribution of sand movement from the port entrance across narrow segments, and results were obtained that dramatically increased the sedimentation rate, approaching the actual sedimentation rate.

Sugawara and Takahashi (2014) focused on topography change of the Sendai plain due to the 2011 Tohoku tsunami, conducted a numerical simulation using a method that utilized the coefficients for pick-up and bed load sediment, which were found using Takahashi et al. (2011) with the method presented by Takahashi et al. (1999), and verified its applicability for calculating topography change due to the 2011 Tohoku tsunami. A comparison was conducted of calculated results and observed values for a vertical cross-section, and it was verified that the calculation was able to provide a good reproduction of the behind seawalls and sandbars. On the other hand, in order to use calculations to

reproduce and deposits with regard to coastal forests, there are still issues in that it is necessary to take into account spatial and temporal changes in the roughness coefficient, and further research is needed on model parameters for applying the sediment transport model to tsunami deposits thinner than 30 cm that are inland.

Sugawara et al. (2014) conducted an examination of topography change of the Sendai plain due to the 2011 Tohoku tsunami. Multiple parametric studies, which included particle size, upper concentration limits for suspended sediment, and other elements, were conducted by using the coefficients for pick-up and bed load sediment, which were found using Takahashi et al. (2011) with the method presented by Takahashi et al. (1999). In addition to a basic setting of 2% for the upper concentration limit for suspended sediment, the examination reviewed limits of 1% and 4%.

Yamashita et al. (2015) performed empirical calculations using the method presented by Takahashi et al. (2011) to examine topography change in Rikuzentakata city due to the 2011 Tohoku tsunami. The upper concentration limit for suspended sediment was set using a relational expression commensurate with current velocity and water depth just as was presented by Imai et al. (2015) (from interview with the authors). The calculation results captured well the distribution trend of and sediment that emerged in the results of field investigations and were able to provide good reproductions of the distribution trends of sediment in sea areas for the extent of topography change, inundation height and the process of tsunami run-up (Figure 8.2.3-5). The calculations for the extent of topography change showed that there was of $2.1 \times 10^6 \text{m}^3$, which was about the same level as the results of field investigations ($1.9 \times 10^6 \text{m}^3$).

Imai et al. (2015) performed numerical calculations using the method presented by Takahashi et al. (2011) to examine topography change in the vicinity of the mouth of the Kitakami river due to the 2011 Tohoku tsunami, and was able to reproduce, for the most part, topography change of cultivated agricultural land (Figure 8.2.3-6). For the upper concentration limit for suspended sediment, a saturated suspended sediment concentration formula was adopted, which is shown below and varies according to the flow conditions according to Sugawara et al. (2014).

$$C_s \approx \frac{\rho_s \rho_w}{\rho_s - \rho_w} \left(\frac{h^{\frac{4}{3}} w_s}{e_s n^2 u^3} - 1 \right)^{-1}$$

where, ρ_s : sand density (kg/m^3), ρ_w : water density (kg/m^3), h : water depth, w_s : sand sedimentation rate (m/s), u : cross-sectional mean current velocity including sand (m/s), n : Manning's roughness coefficient ($\text{m}^{-1/3} \cdot \text{s}$), and e_s : pick-up efficiency.

The configuration when sediment transport was calculated in the previous studies discussed so far regarding the concentration of suspended sediment in seawater during a tsunami have been consolidated in a table (Table 8.2.3-2).

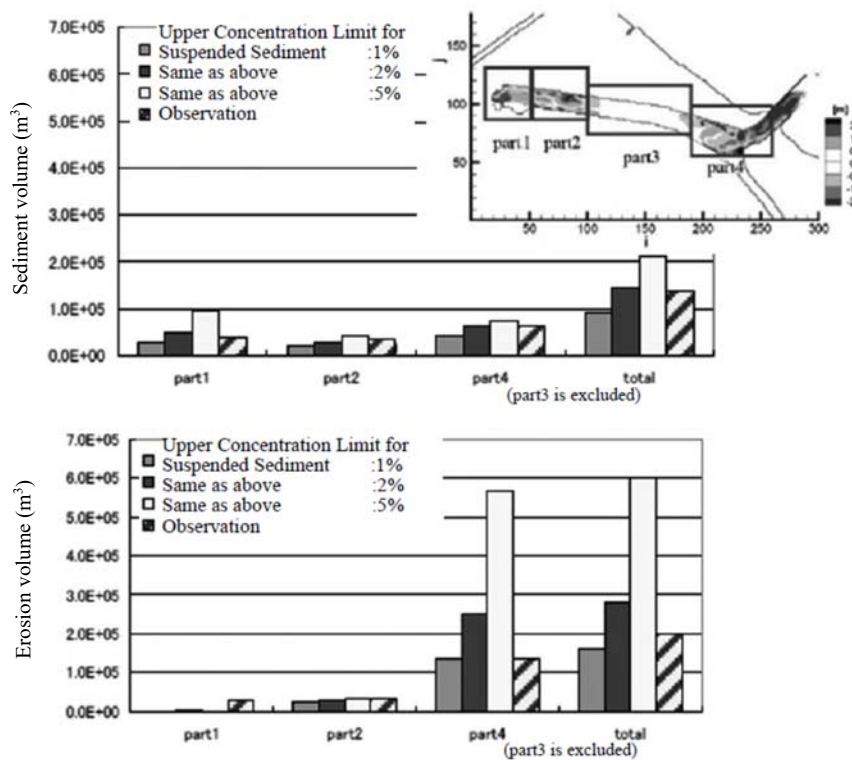


Figure 8.2.3-3 Total result of topography changes per domain (Fujita et al., 2010)

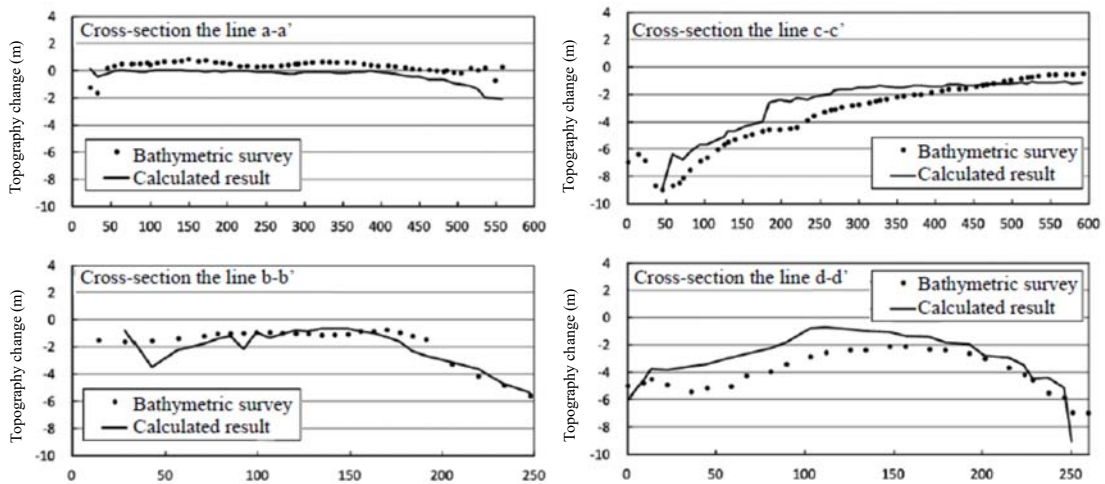
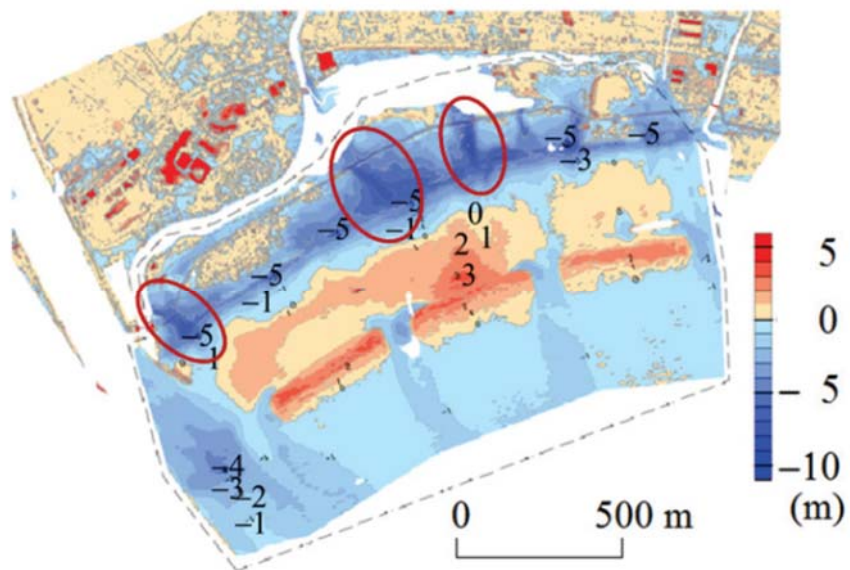
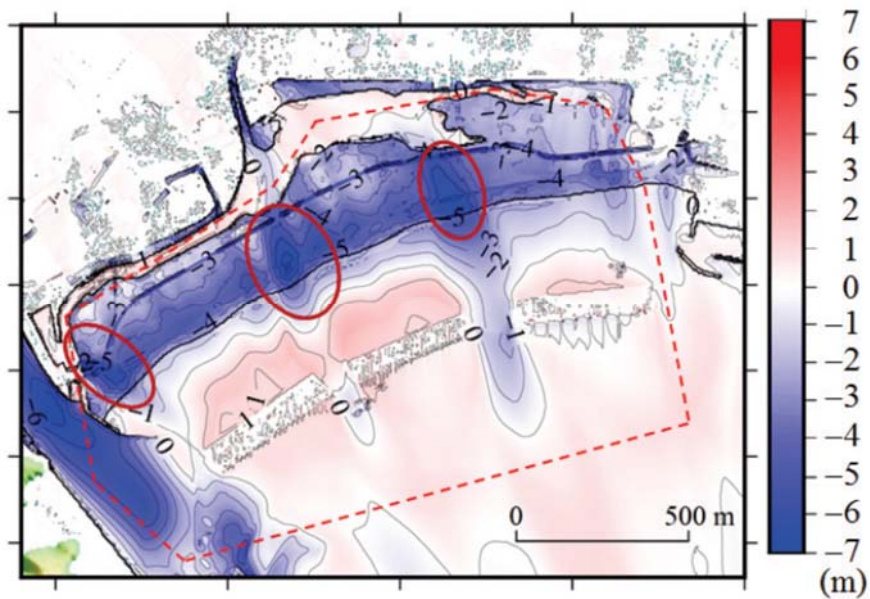


Figure 8.2.3-4 Topography changes of representative cross section (Kondo et al., 2012)

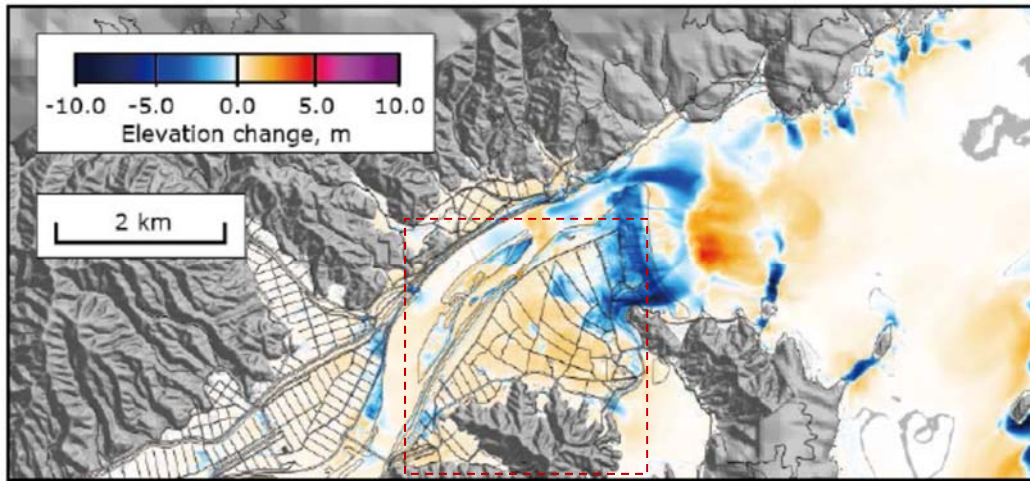


(a) Field survey results (survey in May 2011) (retouch figure by Kato et al., 2012)



(b) Result of calculation

Figure 8.2.3-5 Comparing results of topography changes (Yamashita et al., 2015)



(b) $d=0.267$ mm

* Add the range of the dashed line frame to a figure of Imai et al. (2015)

Figure 8.2.3-6 Maximum topography change distribution around the Kitakami River estuary (Imai et al., 2015)

Table 8.2.3-2 Previous studies on upper concentration limits for suspended sediment

literature	Real scale verification	Sand particle size used for calculation	Calculation grid intervals	Upper concentration limits for suspended sediment	Description on upper concentration limits for suspended sediment
Takahashi et al. (1999)	Kesennuma Bay* ¹	0.2mm	25m	-	-
Tamada et al. (2009)	Kesennuma Bay* ¹	0.001mm-1mm	25m,5m	1%,5%	There was a tendency to overestimate depth to be greater than the actual values when the upper concentration limit for suspended sediment was 5%.
Fujita et al. (2010)	Hachinohe Port* ¹	0.26mm	10.3m	1%,2%,5%	There was good reproducibility when the upper concentration limit for suspended sediment was set at 1% and 2%. An overestimate would result using an upper concentration limit for suspended sediment of 5%.
Kondo et al. (2012)	Miyako Port* ²	0.08mm	10m	1%	The model presented by Takahashi et al. (1999) was able to reproduce with sufficient precision the actual topographical change.
Morishita et al. (2014)	Kesennuma Bay* ¹	0.3mm	10m	1% Variable	$\alpha \times \sqrt{U^2 + V^2}$ U and V are average current velocity(m/s) When current velocity was 10m/s, α was set with 0.01 so that upper concentration limit for suspended sediment became 0.1.
Sugawara and Takahashi (2014)	Sendai Plain Around Natori River* ²	0.25mm	-	1%	A comparison was conducted of calculated results and observed values for a vertical cross-section, and it was verified that the calculation was able to provide a good reproduction of the behind seawalls and sandbars.
Sugawara et al. (2014)	Sendai Plain* ²	0.166mm 0.267mm 0.394mm	Minimum:5m	1%,2%,4%	The parameter study that changed sand particle size and suspended sediment concentration limits was carried out, and topography change was reproduced well when an upper concentration limit for suspended sediment was set in 2%.
Yamashita et al. (2015)	Rikuzentakata City Hirota Bay* ²	0.267mm	-	Variable	A tendency of the topography amount of change was reproduced well. By the method of Takahashi et al. (1999), pick-up is remarkably excessive, and the reproduction of the topography change is difficult.
Imai et al. (2015)	Kitakami Rive* ²	0.166mm 0.267mm 0.394mm	Minimum:5m	Variable	Topography change was reproduced well, by using the numerical simulation model that upper concentration limit for suspended sediment was set by a function depending on the current velocity and the water depth.

*1: Topography change caused by the 1960 Chile tsunami, *2: Topography change caused by the 2011 off the Pacific coast of Tohoku Earthquake tsunami.

8.3. Evaluation of debris

8.3.1. Specifics of equations for calculating the impact force attributable to debris

Table 8.3.1-1 shows a classification of previously proposed equations for calculating the impact force of debris.

Table 8.3.1-1 Classification of equations for calculating the impact force of debris

Author name	Type of debris	Equations of impact force of tsunami debris
Matsutomi et al. (1999)	Wood (Cylinder)	$F_m / (\gamma D^2 L) = (1.2 \sim 1.5) C_{MA} \left\{ v_{A0} / (gD)^{0.5} \right\}^{1.2} (\sigma_f / \gamma L)^{0.4}$ <p>F_m: Impact force, γ: Unit weight of drift wood, D: Diameter of wood, L: Length of wood, g: Acceleration of gravity, C_{MA}: Apparent mass coefficient (Considering buffering function of water), v_{A0}: Impact velocity, σ_f: Yield stress of wood</p>
Ikeno and Tanaka (2003)	Wood (Cylinder, Prism, Sphere)	$F_H / (gM) = S \cdot C_{MA} \cdot \left\{ V_H / (g^{0.5} D^{0.25} L^{0.25}) \right\}^{2.5}$ <p>F_H: Impact force, g: Acceleration of gravity, M: Weight of debris, S: Coefficient (=5.0), C_{MA}: Added-mass coefficient, V_H: Velocity of debris, D: Diameter of debris (In case of a rectangular column, the square section side length), L: Length of debris</p>
Japan Road Association(2012)	Drift wood, etc.	$P = 0.1Wv$ <p>P: Impact force, W: Weight of transport object, v: Surface flow velocity</p>
FEMA (2012)	Wood Container	$F_i = 1.3u_{\max} \sqrt{km_d(1+c)}$ <p>F_i: Impact force, c: Added-mass coefficient, u_{\max}: Maximum flow velocity of the fluid, m_d, k: Mass and effective stiffness of debris</p>
Mizutani et al. (2005)	Container	$F_m = 2\rho_w \eta_m B_c V_x^2 + \left(\frac{WV_x}{gdt} \right), V_x \cong C_x = 2\sqrt{g\eta_m}$ <p>F_m: Impact force, g: Acceleration of gravity, W: Weight of container, B_c: Width of container, η_m: Maximum water level of run-up tsunami, dt: Impact time, ρ_w: Density of water, V_x: Drifting container velocity, C_x: Flow velocity of run-up tsunami</p>
Arikawa and Washizaki (2010)	Container Drift wood	$F = \gamma_p \chi^{\frac{2}{5}} \left(\frac{5}{4} \tilde{m} \right)^{\frac{3}{5}} v^{\frac{6}{5}} \chi = \frac{4\sqrt{a}}{3\pi} \frac{1}{k_1 + k_2}, k = \frac{(1-v^2)}{\pi E}, \tilde{m} = \frac{m_1 m_2}{m_1 + m_2}$ <p>a: One half of radius of impact surface (Here, it is $1/4$ of the average of the longitudinal and lateral lengths of the container impact surface), E: Young's modulus of concrete, v: Poisson ratio, m: mass, v: Impact velocity, γ_p: Energy damping effect by plastic, Subscript 1: Collision body, Subscript 2: Colliding body</p>
Japan Bridge Engineering Center (1978)	Ship	$F = \frac{WV^2}{4gD}$ <p>F: Impact force, W: Weight of impact ship, V: Impact velocity, D: Stopping distance of impact ship</p>

8.3.2. Verification of the validity of impact force calculation formulae

8.3.2.1. Examination overview

Using the results of hydraulic model experiments for large debris based upon Takabatake et al. (2015), an examination was conducted on the applicability of previous impact force calculation formulae and the properties of impact force. Aerial experiments and underwater experiments were used for the examination which focused on logs and automobiles as the debris.

8.3.2.2. Experiment overview

(1) Debris

For the debris, in addition to three types of logs, which are given in Table 8.3.2-1, the subcompact automobile, which is shown in Figure 8.3.2-1, was used.

Table 8.3.2-1 Debris using for experiment (log)

Type	Length	Diameter	Mass	Modulus of elasticity
Cedar	1m	0.380m	72kg	9.1 kN/mm ²
	2m		155kg~158kg	
Pine	2m	0.435m	178kg~181kg	11.2 kN/mm ²



<u>Specifications</u>
Length: 3,925mm
Width: 1,395mm
Height: 1,475mm
Mass: 320kg
Remarks: Engine and glass which do not influence the strength are removed

Figure 8.3.2-1 Debris using for experiment (car) (A simple configuration of Takabatake et al (2015))

(2) Measurement of impact force

For the experiment, the reactive force was measured by using steel plates to which steel rods were attached that were capable of measuring axial strain. To convert the reactive force to impact force, first, aerial experiments were conducted to find the inertial force (impact force) of an impactor by means of an accelerometer attached to the impactor (debris), and next, the conversion

coefficient was obtained between the inertial force and reactive force for the steel plate so as to calculate the impact force during underwater experiments.

(3) Empirical results

1) Aerial experiments

The distinctive features of impact force of debris during the aerial experiments are given below.

- The impact force of logs (wood) increased linearly vis-a-vis the impact velocity, and there was a trend whereby the smaller the impact angle (angle formed by the steel plate), the smaller the impact force (Figure 8.3.2-3).
- The impact force of automobiles was 1/10 or less than that of logs, and the impact force increased linearly at impact velocities between 0.2m/s and 0.4m/s (Figure 8.3.2-5).

2) Underwater experiments

The distinctive features of impact force during the underwater experiments are given below.

- The relationship between the impact velocity and impact force of logs (wood) is different from the trend observed during aerial experiments (Figure 8.3.2-4).
- The impact force of automobiles increased almost linearly with respect to the impact velocity, and if the storage water level was the same, the impact velocity or impact force would increase at the higher initial water level (Figure 8.3.2-5).
- As for the effect of water when debris strikes a structure, almost no additional mass effect (effect of impact force increase) was observed, and there were many cases where a cushion effect (effect of impact force decrease) was noticeably apparent (Figure 8.3.2-2).

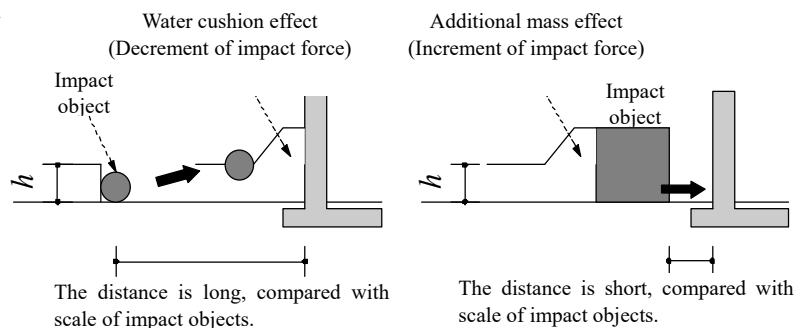


Figure 8.3.2-2 The effect of water when the debris impacts with a structure

8.3.2.3. Impact force attributable to logs (wood)

The results of aerial experiments and underwater experiments were used to examine the applicability of previous impact force calculation formulae.

(1) Physical properties of logs

The physical properties of logs were examined for both cases where previous settings (catalog values) were used, and cases where actually-measured physical properties were used (Table 8.3.2-2).

Table 8.3.2-2 Physical property values of logs

(1) Previous settings (catalog values)

	Modulus of elasticity* ¹ E (kN/mm ²)	Diameter D (m)	Length L (m)	Mass m (kg)	Density ρ (kg/m ³)	Effective stiffness* ² k (kN/m)
Cedar	7.1	0.380	2.0	156	687.8	2.4×10^3
			1.0	72	634.9	
Pine	11.0	0.435	2.0	179	602.3	

*1: Shimazu et al. (2001)

*2: FEMA (2012)

(2) Actually-measured physical properties

	Modulus of elasticity E (kN/mm ²)	Diameter D (m)	Length L (m)	Mass m (kg)	Density ρ (kg/m ³)	Effective stiffness* ³ k (kN/m)
Cedar	9.1	0.380	2.0	156	687.8	$\frac{E \pi D^2}{L 4}$
			1.0	72	634.9	
Pine	11.2	0.435	2.0	179	602.3	

*3: FEMA (2012)

(2) Previous impact force calculation formulae

For a comparison with empirical results, the impact force calculation formulae were used as presented by Matsutomi (1999), Ikeno and Tanaka (2003), Arikawa and Washizaki (2010), and FEMA (2012), which are calculations that focus on wood as the impactor and addressed phenomena similar to the phenomena in this experiment. The coefficients in the calculation formulae were set as indicated in Tables 8.3.2-3 and 8.3.2-4.

For the flow velocity in the calculation formula presented by FEMA (2012), the velocity (impact velocity) at the moment when wood strikes the abutment was used.

Table 8.3.2-3 Setting of coefficients in the calculation formulae (Aerial experiments of logs)

Calculation formulae of impact force	Coefficients	Setting value	Remarks
Matsutomi (1999)	C_{MA}	1.0	Aerial experiments
Ikeno and Tanaka (2003)	S	5.0	
	C_{MA}	1.0	Aerial experiments
Arikawa and Washizaki (2010)	γ_p	0.25	
	ν	0.4	
FEMA(2012)	C	0	Aerial experiments

Table 8.3.2-4 Setting of coefficients in the calculation formulae (Underwater experiments of logs)

Calculation formulae of impact force	Coefficients	Setting value	Remarks
Matsutomi (1999)	C_{MA}	1.7	Value of surge
Ikeno and Tanaka (2003)	S	5.0	
	C_{MA}	1.5	Horizontal cylinder
Arikawa and Washizaki (2010)	γ_p	0.25	
	ν	0.4	
FEMA(2012)	C	0.3	

(3) Comparison of impact force estimation equations and empirical results

1) Aerial experiments using logs

Figure 8.3.2-4 is a comparison of empirical results with impact force calculation formulae for a case where previous settings (catalog values) were used for the relationship of impact force and impact velocity in aerial experiments using logs. The impact angle in the empirical results was 90° (vertical) for both. The distinctive features of each calculation formula are given below.

- The estimation formulae presented by Arikawa and Washizaki (2010) and Matsutomi (1999) coincide well with the empirical results, and there is no significant difference in the impact force between the case where previous settings were used and the case where measured physical properties were used.
- The estimation formula presented by FEMA (2012) provided somewhat smaller results in comparison to the empirical results for a case where previous settings were used. On the other hand, when measured physical properties were used, the impact force varied significantly depending on the value of the effective axial rigidity.
- The estimation formula presented by Ikeno and Tanaka (2003) tended to have smaller

results than the empirical results in all cases.

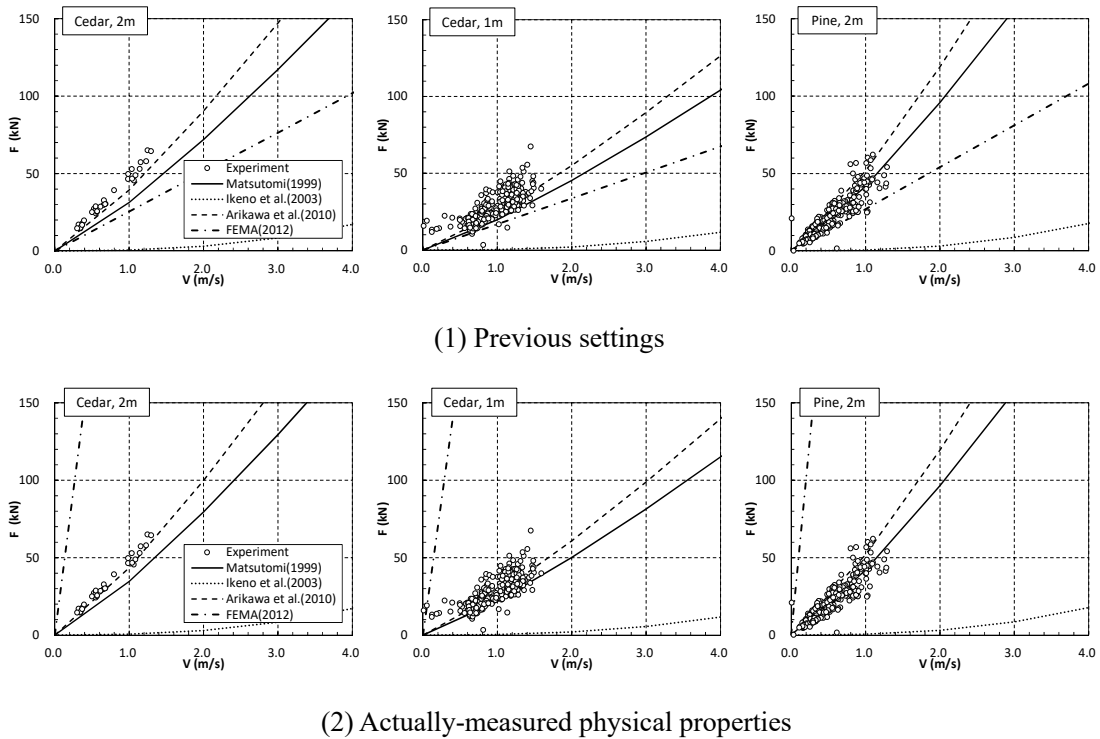


Figure 8.3.2-3 Comparison between impact force calculation formulae and empirical results (Aerial experiments of logs)

2) Underwater experiments using logs

Figure 8.3.2-3 is a comparison of empirical results with impact force calculation formulae for a case where previous settings (catalog values) were used for the relationship of impact force and impact velocity in underwater experiments using logs. The impact angle in the empirical results was 0° (horizontal) for all cases. The distinctive features of each calculation formula are given below.

- The impact force found using the calculation formula presented by Ikeno and Tanaka (2003) coincided well with the empirical results.
- The impact force found using the calculation formulae presented by Matsutomi (1999), Arikawa and Washizaki (2010) and FEMA (2012) was quite greater than that in the empirical results.

However, it needs to be kept in mind that, in contrast to the empirical results which show a impact force using a impact angle of 0° (horizontal), the calculation formulae presented by Matsutomi (1999) as well as Arikawa and Washizaki (2010) covered a impact angle of 90° (vertical), and a impact angle of 90° (vertical) was used for the effective axial rigidity as presented by FEMA (2012).

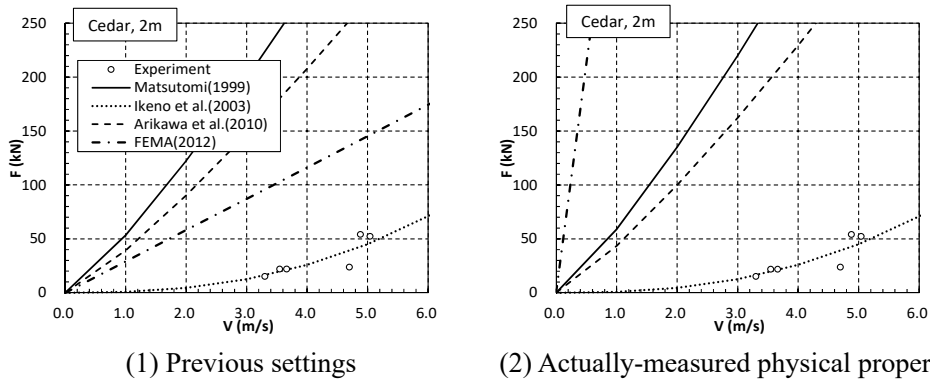


Figure 8.3.2-4 Comparison between impact force calculation formulae and empirical results (Underwater experiments of logs)

8.3.2.4. Impact force attributable to automobiles

The results of aerial experiments and underwater experiments were used to examine the applicability of previous impact force calculation formulae.

(1) Previous impact force calculation formulae

Because there were no previous impact force calculation formulae that covered automobiles, the applicability of FEMA (2012), which has a comparatively broad scope of applicability, was examined as a impact force calculation formula (see Appendix Section 8.3.1 for specifics pertaining to the calculation formula).

For the effective axial rigidity k in the FEMA (2012) calculation formula, the two types of settings given in Table 8.3.2-5 were used. Also, the additional mass coefficient C for cases where aerial experiments were conducted was 0.0. The additional mass coefficient C for cases where underwater experiments were conducted took into account the estimated values according to FEMA (2012) ranging from 0.0 to 0.3, and two settings were used, 0.0 and 0.3.

Table 8.3.2-5 Setting of coefficients in the calculation formulae (car)

Calculation formulae of impact force	Effective stiffness k (kN/m)	Remarks
FEMA(2012)	1.5×10^6	Value of 20ft container by FEMA(2012)
	1.35×10^2	Value of static load test

(2) Comparison of impact force estimation equation and empirical results

Figure 8.3.2-5 is a comparison of the impact force calculation formula and empirical results

for the relationship of impact force and impact velocity in underwater experiments using automobiles.

1) Aerial experiments using automobiles

The features of the FEMA (2012) calculation formula are given below.

- For the impact force in a case where the value was used for axial rigidity of a 20 foot container according to FEMA (2012), calculation results that greatly exceeded the empirical results were obtained.
- For the impact force in a case where the value was used for axial rigidity which was determined based upon static load tests, the calculation results somewhat exceeded the empirical results.
- Application of impact force calculation formulae to automobiles is difficult because there are almost no previous references to effective axial rigidity or elasticity coefficient.

2) Underwater experiments using automobiles

The features of the FEMA (2012) calculation formula are given below.

- For the impact force in a case where the value was used for axial rigidity of a 20 feet container according to FEMA (2012), calculation results that exceeded the empirical results were obtained.
- For the impact force in a case where the value was used for axial rigidity which was determined based upon static load tests, the calculation results were below the empirical results.
- Application of impact force calculation formulae to automobiles is difficult because there are almost no previous references to effective axial rigidity or elasticity coefficient.

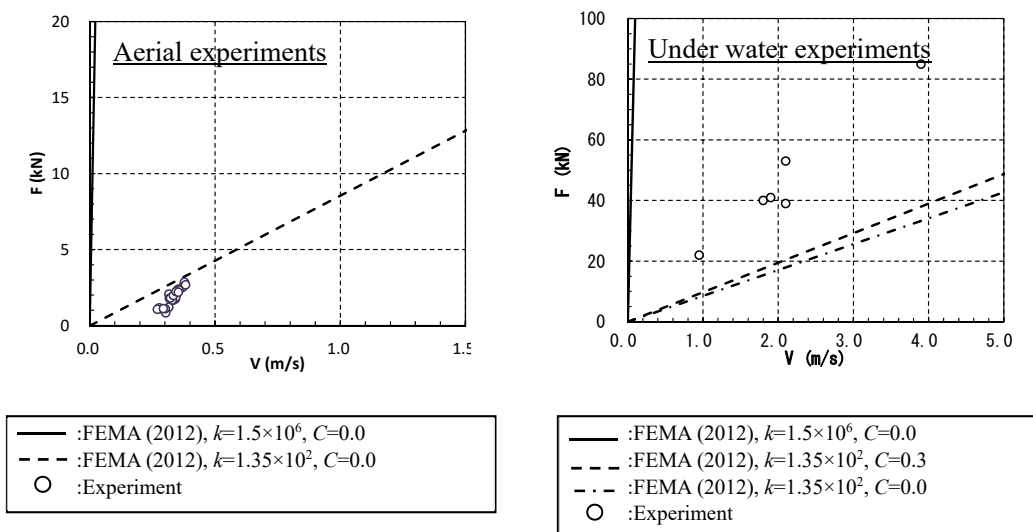


Figure 8.3.2-5 Comparison between impact force calculation formulae and empirical results (car)

8.3.3. Previous analysis examples of methods for analyzing debris

Examples of previous analyses of methods for analyzing debris were consolidated. When the previous analysis examples were broadly classified, they were separated into methods using the results of tsunami calculations in a plane two-dimensional model based upon the shallow water equation to analyze the movement of debris, and methods expressing debris as a solid phase to simultaneously calculate mutual interference with fluid (cross-sectional two-dimensional model or three-dimensional model).

(1) Methods using the results of tsunami calculations based upon the shallow water equation to analyze the movement of debris (plane two-dimensional model)

- Goto (1983)
- Fujii et al. (2005), and Fujii and Imamura (2010)
- Kobayashi et al. (2005), Honda et al. (2009), Hashimoto et al. (2009), and Hashimoto et al. (2010)

Table 8.3.3-1 shows representative examples of previous analyses with the method using the results of tsunami calculations based upon the shallow water equation to analyze the movement of debris.

(2) Methods expressing debris as a solid phase to simultaneously calculate mutual interference with fluid (cross-sectional two-dimensional or three-dimensional model)

- Kawasaki et al. (2006)
- Kawasaki and Hakamada (2007)
- Yoneyama et al. (2008)
- Yoneyama and Nagashima (2009)
- Goto et al. (2009)
- Ikeda and Arikawa (2014)

Table 8.3.3-2 shows representative examples of previous analyses with the method expressing debris as a solid phase to simultaneously calculate mutual interference with fluid.

In addition to the calculation of tsunami debris, Fujii and Imamura (2010) put together disaster scenarios and procedures for estimating damage due to tsunami debris.

Based upon the aforementioned examples of analyses of tsunami debris, it may be said that plane two-dimensional analyses are practical for calculating the trajectory of debris across a wide area, and three-dimensional analyses and cross-sectional two-dimensional analyses are effective means for ascertaining the behavior of debris when a tsunami strikes and the circumstances of

impacts with structures.

Table 8.3.3-1 Representative examples of previous analysis with the method of solving the behavior of debris using the result of the tsunami calculation based on shallow water equation

Author name	Objects	Analysis model	Overview of methods for analyzing debris	Validity of the verification method
Fujii et al. (2005)	Ship	Two-dimensional model	<ul style="list-style-type: none"> • Ship is modeled by distinct element method (DEM) and ship's behavior is calculated by 6 degree of freedom momentum equation on translation and rotation. • Morrison formula is applied to the fluid force required for the calculation of the drift of the ship. • Uses the water level and flow velocity of tsunami analysis by shallow water equation. 	Comparison of the hydraulic model experiment
Honda et al. (2009)	Ship	Two-dimensional model	<ul style="list-style-type: none"> • For the calculation of tsunami flow condition, use storm surge and tsunami simulator (STOC). • The momentum equation concerning the drifting of the ship is formulated assuming that the main movement is front and rear, right and left, and yaw direction, and a hull moving coordinate system whose origin is the hull center of gravity is used. • The fluid force required to calculate the drift of a ship is based on the extension of Morrison equation. • Consider impact of debris with the ground and buildings and mutual impact of debris. 	Test calculation and applied to the actual terrain

Table 8.3.3-2 Representative examples of previous analysis with the method of expressing debris in solid phase to calculation mutual interference with fluid simultaneously

Author name	Objects	Analysis model	Overview of methods for analyzing debris	Validity of the verification method
Yoneyama and Nagashima (2009)	Wood	Three-dimensional model	<ul style="list-style-type: none"> • Three-dimensional Numerical Analysis Method considering translational 3 DOF (degree of freedom) and 3 DOF rotation. • The fundamental equation of the fluid is the same as Yoneyama et al. (2008). • Set the inertia main axis coordinate system with the center of gravity of the rigid body as the origin and Formulation of the momentum equation of the debris center of gravity and the momentum equation of the rotary motion about the center of gravity of the debris. • The fluid force experienced by the debris also takes into consideration the pressure and adhesive force and the impact of the debris against the wall surface. 	Comparison of the hydraulic model experiment by Ikeno et al. (2003)
Goto et al. (2009)	Container	Three-dimensional model	<ul style="list-style-type: none"> • Fluid analysis uses the MPS method, and the momentum equation uses the Navier-Stokes equation. • The container constitutes a plurality of solid phase particles by a rigid body connected model. • The fluid acting on the container is calculated by incorporating the rigid constituent particles together with the fluid particles into the intergranular interaction model. 	Comparison of the hydraulic model experiment by Arikawa et al. (2007)

[Appendix 8 References]

Arikawa, T., M. Ikebe, F. Yamada, K. Shimosako and F. Imamura (2005) Large Model Test of Tsunami Force on a Revetment and on a Land Structure, Annual Journal of Coastal Engineering, JSCE, Vol. 52, pp. 746-750 (in Japanese).

<http://library.jsce.or.jp/jsce/open/00008/2005/52-0746.pdf>

Arikawa, T. and M. Washizaki (2010) Large Scale Tests on Concrete Wall Destruction by Tsunami with Driftwood, Journal of JSCE, Ser. B2 (Coastal Engineering), Vol. 66, pp. 781-785 (in Japanese).

https://www.jstage.jst.go.jp/article/kaigan/66/1/66_1_781/_pdf

Arikawa, T., T. Ikeda and K. Kubota (2014) Experimental Study on Scour behind Seawall due to Tsunami Overflow, Journal of JSCE, Ser. B2 (Coastal Engineering), Vol. 70, pp. 926-930 (in

- Japanese).
- https://www.jstage.jst.go.jp/article/kaigan/70/2/70_I_926/_pdf
- Arimitsu, T., K. Ooe and K. Kawasaki (2012) Proposal of Evaluation Method of Tsunami Wave Pressure Using 2D Depth-Integrated Flow Simulation, Journal of JSCE, Ser. B2 (Coastal Engineering), Vol. 68, pp. 781-785 (in Japanese).
- https://www.jstage.jst.go.jp/article/kaigan/68/2/68_I_781/_pdf
- Asakura, R., K. Iwase, T. Ikeya, M. Takao, T. Kaneto, N. Fujii and M. Omori (2000) An Experimental Study on Wave Force Acting on On-Shore Structures due to Overflowing Tsunamis, Proceedings of Coastal Engineering, JSCE, Vol. 47, pp. 911-915 (in Japanese).
- <http://library.jsce.or.jp/jsce/open/00008/2000/47-0911.pdf>
- Asakura, R., K. Iwase, T. Ikeya, M. Takao, T. Kaneto, N. Fujii and M. Ohmori (2002) The Tsunami Wave Force Acting on Land Structures, Proceedings of 28th International Conference on Coastal Engineering, pp. 1191-1202.
- Ashida, K. and M. Michiue (1972) Study on hydraulic resistance and bed-load transport rate in alluvial streams, Proceedings of the Japan Society of Civil Engineers, Volume 1972 (1972) Issue 206, pp. 59-69 (in Japanese).
- <http://library.jsce.or.jp/jsce/open/00037/206/206-0059.pdf>
- Building Research Institute (2012) 2011 Report on Investigation of Great East Japan Earthquake Damage (in Japanese).
- <http://www.kenken.go.jp/japanese/contents/topics/20110311/0311report.html>
- Cabinet Office Japan (2005) Guideline for Buildings to Evacuate from Tsunami (in Japanese).
- <http://www.bousai.go.jp/kohou/oshirase/h17/pdf/050323shiryoku2.pdf>
- Dames and Moore (1980) Design and Construction Standards for Residential Construction in Tsunami-Prone Areas in Hawaii, prepared by Dames & Moore for the Federal Emergency Management Agency, Washington D.C.
- Disaster Prevention Working Group, Ports Subcommittee, Council for Transport Policy under the Ministry of Land, Infrastructure, Transport and Tourism (2011) Comprehensive Approach to Tsunami Countermeasures for Harbours and Ports (Interim Report) (in Japanese).
- <http://www.mlit.go.jp/common/000149434.pdf>
- Disaster Prevention Working Group, Ports Subcommittee, Council for Transport Policy under the Ministry of Land, Infrastructure, Transport and Tourism (2012) Approach to Tsunami Countermeasures for Harbours and Ports (in Japanese).
- <http://www.mlit.go.jp/common/000214200.pdf>
- Federal Emergency Management Agency (2012) Guidelines for Design of Structures for Vertical Evacuation from Tsunamis, Second Edition, FEMA P-646.
- Fire and Disaster Management Agency (2009) Report of Tsunami inundation measures for the

- Facilities dealing with hazardous materials (in Japanese).
http://www.fdma.go.jp/neuter/topics/houdou/h21/2105/210526-1houdou/02_stunami_houkokusyo.pdf
- Fujii, N., M. Ohmori, M. Takao, S. Kanayama and H. Ohtani (1998) On the Deformation of the Sea Bottom Topography due to Tsunami, Proceedings of Coastal Engineering, JSCE, Vol. 45, pp. 376-380 (in Japanese).
<http://library.jsce.or.jp/jsce/open/00008/1998/45-0376.pdf>
- Fujita, N., K. Inagaki, N. Fujii, M. Takao and T. Kaneto (2010) PROCEEDINGS OF CIVIL ENGINEERING IN THE OCEAN, Vol. 26, pp. 213-218 (in Japanese).
- Fukui, Y., H. Shiraishi, M. Nakamura and Y. Sasaki (1962) Proceedings of Coastal Engineering, JSCE, Volume 9 (1962), pp. 50-54 (in Japanese).
https://www.jstage.jst.go.jp/article/proce1955/9/0/9_0_50/_pdf
- Gotoh, H. , H. Ikari, K. Haraguchi, H. Nakajima, K. Tonono and T. Ishii (2013) Development of Numerical Wave Flume by Particle Method for Simulating Tsunami-Overtopping induced Failure of Composite Breakwater and its Prevention Work, Journal of JSCE, Ser. B2 (Coastal Engineering), Vol. 69, pp. 881-885 (in Japanese).
https://www.jstage.jst.go.jp/article/kaigan/69/2/69_I_881/_pdf
- Homma, M (1940) Japan Society of Civil Engineering (JSCE), Civil Engineering, Vol. 26(6), pp. 635-645 (in Japanese).
<http://library.jsce.or.jp/jsce/open/00034/26-06/26-6-12899.pdf> ,
 and Civil Engineering, Vol. 26(9), pp. 849-862 (in Japanese).
<http://library.jsce.or.jp/jsce/open/00034/26-09/26-9-12910.pdf>
- Iizuka, H. and H. Matsutomi (2000) Damage due to the Flooding Flow of Tsunami, Proceedings of Coastal Engineering, JSCE, Vol. 47, pp. 381-385 (in Japanese).
<http://library.jsce.or.jp/jsce/open/00008/2000/47-0381.pdf>
- Ikeno, M. and H. Tanaka (2003) Experimental Study on Impulse Force of Drift Body and Tsunami Running Up to Land, Proceedings of Coastal Engineering, JSCE, Vol. 50, pp. 721-725 (in Japanese).
<http://library.jsce.or.jp/jsce/open/00008/2003/50-0721.pdf>
- Ikeno, M., M. Matsuyama, T. Sakakiyama and K. Yanagisawa (2005) Experimental Study on Tsunami Force Acting on Breakwater with Soliton Fission and Breaking of Split Waves, Annual Journal of Coastal Engineering, JSCE, Vol. 52, pp. 751-755 (in Japanese).
<http://library.jsce.or.jp/jsce/open/00008/2005/52-0751.pdf>
- Ikeno, M., M. Matsuyama, T. Sakakiyama and K. Yanagisawa (2006) Experimental Study on Force of Tsunami with Soliton Fission Running up on Land, Annual Journal of Coastal Engineering, JSCE, Vol. 53, pp. 776-780 (in Japanese).

- <http://library.jsce.or.jp/jsce/open/00008/2006/53-0776.pdf>
- Ikeno, M., T. Yoshii, M. Matsuyama and N. Fujii, (2009) Estimation of Pickup Rate of Suspended Sand by Tsunami Experiment and Proposal of Pickup Rate Formula, Journal of JSCE, Ser. B2 (Coastal Engineering), Vol. 65, pp. 506-510 (in Japanese).
https://www.jstage.jst.go.jp/article/kaigan/65/1/65_1_506/_pdf
- Imai, K., D. Sugawara, T. Takahashi, S. Iwama and H. Tanaka (2015) Numerical Study for Sediment Transport Due to Tsunami Around the Kitakami River Mouth, Journal of JSCE, Ser. B2 (Coastal Engineering), Vol. 71, pp. 247-252 (in Japanese).
https://www.jstage.jst.go.jp/article/kaigan/71/2/71_I_247/_pdf
- Ishida, N., H. Moritani, H. Nakamura, T. Iijima and H. Kawauchi (2014) Applicability of Water Depth Coefficient in Evaluation for Tsunami Wave Force Acting on Seawall, NRA Technical Report Series, NTEC-2014-4001 (in Japanese).
<http://www.nsr.go.jp/data/000167078.pdf>
- Japan Bridge Engineering Center (1978) Technical standards for Honshu-Shikoku Bridge Substructures, pp. 9-19-9-20 (in Japanese).
- Japan Road Association (2012) Road bridge specification book and manual, ISBN 978-4-88950-265-7, 71p. (in Japanese).
- Kihara, N., D. Takabatake, T. Yoshii, M. Ikeno, K. Ota and N. Tanaka (2012) Tsunami fluid force on land structures (Part I) - Numerical study for structures with finite width under non-overflow condition-, CRIPI Research Report, N12010 (in Japanese).
<http://cripi.denken.or.jp/jp/kenkikaku/report/download/ooU04IL6eIPGNd5C3JYuRjZ9bZairlxW/N12010.pdf>
- Kihara, N., H. Kaida, Y. Miyagawa, D. Takabatake, A. Shibayama, Y. Niida and M. Matsuyama (2015) Development of tsunami fragility evaluation methods by large scale experiments (Part I)- Validation of evaluation methods of tsunami-induced hydrodynamic load -, CRIPI Research Report, O15002 (in Japanese).
<http://cripi.denken.or.jp/jp/kenkikaku/report/download/FTu598IdJ9vijnAAr7V0dAwWo6PUPh9l/O15002.pdf>
- Kobayashi, A., Y. Oda, T. Toe, M. Takao and N. Fujii (1996) Study on Sediment Transport due to Tsunamis, Proceedings of Coastal Engineering, JSCE, Vol. 50, pp. 721-725 (in Japanese).
<http://library.jsce.or.jp/jsce/open/00008/1996/43-0691.pdf>
- Kondo, T., T. Morimoto, N. Fujimoto, K. Tonono and T. Shikata, (2012) Accuracy Evaluation of Numerical Simulations to Calculate Sediment Transport in Harbor due to Tsunami, Journal of JSCE, Ser. B2 (Coastal Engineering), Vol. 68, pp. 396-400 (in Japanese).
https://www.jstage.jst.go.jp/article/kaigan/68/2/68_I_396/_pdf
- Kuriki, M., T. Suetsugu, H. Umino, Y. Tanaka and H. Kobayashi (1996) Flood simulation manual

- (draft). Guide for simulation and verification of new model, Ministry of Construction Public Works Res. Inst. S, No. 3400 (in Japanese).
- Matsutomi, H. (1999) A PRACTICAL FORMULA FOR ESTIMATING IMPULSIVE FORCE DUE TO DRIFTWOODS AND VARIATION FEATURES OF THE IMPULSIVE FORCE, *Doboku Gakkai Ronbunshu*, Volume 1999 (1999) Issue 621, pp. 111-127 (in Japanese).
https://www.jstage.jst.go.jp/article/jscej1984/1999/621/1999_621_111/_pdf/-char/en
- Ministry of Land, Infrastructure, Transport and Tourism, Ports and Harbours Bureau (2013)
<http://www.mlit.go.jp/common/001114049.pdf>
- Ministry of Land, Infrastructure, Transport and Tourism, Tohoku Development Bureau (2011) Report of the damage situation of the outside harbor facilities at Sendai-Shiogama Port (in Japanese).
- Ministry of Transport (1961) Collection of Chilean seismic sea wave documents around the Hachinohe Port (in Japanese).
<http://tsunami-dl.jp/document/060>
- Mizutani, N., Y. Takagi, K. Shiraishi, S. Miyajima and T. Tomita (2005) Study on Wave Force on a Container on Apron due to Tsunamis and Collision Force of Drifted Container, *Annual Journal of Coastal Engineering, JSCE*, Vol. 52, pp. 741-745 (in Japanese).
<http://library.jsce.or.jp/jsce/open/00008/2005/52-0741.pdf>
- Mizutani, S. and F. Imamura (2000) Hydraulic Experimental Study on Wave Force of a Bore Acting on a Structure, *Proceedings of Coastal Engineering, JSCE*, Vol. 47, pp. 946-950 (in Japanese).
<http://library.jsce.or.jp/jsce/open/00008/2000/47-0946.pdf>
- Mizutani, S. and F. Imamura (2002) Design of Coastal Structure Including the Impact and Overflow on Tsunamis, *Proceedings of Coastal Engineering, JSCE*, Vol. 49, pp. 731-735 (in Japanese).
<http://library.jsce.or.jp/jsce/open/00008/2002/49-0731.pdf>
- Morishita, Y. and T. Takahashi (2014) Accuracy improvement of movable bed model for tsunamis by applying for Kesenuma bay when the 2011 Tohoku tsunami arrived, *Journal of JSCE, Ser. B2 (Coastal Engineering)*, Vol. 70, pp. 491-495 (in Japanese).
https://www.jstage.jst.go.jp/article/kaigan/70/2/70_I_491/_pdf
- Nakamura, T., Y. Nezasa and N. Mizutani (2013) Application of Coupled Fluid-Structure-Sediment Interaction Numerical Model to Tsunami-Induced Local Scouring Around a Movable Inland Structure, *Journal of Japan Society of Civil Engineers, Ser. B3 (Ocean Engineering)*, Volume 69 (2013) Issue 2, pp. I_503-I_508 (in Japanese).
https://www.jstage.jst.go.jp/article/jscejoe/69/2/69_I_503/_pdf/-char/en
- Nakamura, T. and N. Mizutani (2014) Numerical Analysis of Tsunami Overflow Over a Coastal Dike and Local Scouring at the Toe of Its Landward Slope, *Journal of Japan Society of Civil Engineers, Ser. B3 (Ocean Engineering)*, Volume 70 (2014) Issue 2, pp. I_516-I_521 (in Japanese).

- https://www.jstage.jst.go.jp/article/jscejoe/70/2/70_I_516/_pdf/-char/ja
- Nakamura, T., K. Hibino, Y. H. Cho, N. Mizutani and Y. Kotake (2015) Numerical Simulation Of Local Scouring At The Landward Tow Of Coastal Dikes Due To The Great East Japan Earthquake Tsunami And The Effectiveness Of Its Countermeasures, Journal of JSCE, Ser. B2 (Coastal Engineering), Vol. 71, pp. 1099-1104 (in Japanese).
- https://www.jstage.jst.go.jp/article/kaigan/71/2/71_I_1099/_pdf
- National Institute for Land and Infrastructure Management(2012) Practical Guide on Requirement for Structural Design of Tsunami Evacuation Buildings, TECHNICAL NOTE National Institute for Land and Infrastructure Management No. 673 (in Japanese).
- <http://www.nilim.go.jp/lab/bcg/siryounn/tnn0673pdf/ks0673.pdf>
- Noguchi, K., S. Sato and S. Tanaka (1997) Large-scale Experiments on Tsunami Overtopping and Bed Scour around Coastal Revetment, Proceedings of Coastal Engineering, JSCE, Vol. 44, pp. 296-300 (in Japanese).
- <http://library.jsce.or.jp/jsce/open/00008/1997/44-0296.pdf>
- Omori, M., N. Fujii, O. Kyouta, M. Takao, T. Kaneto and T. Ikeya (2000) Numerical Simulation of Water Level, Flow Velocity and the Wave Force of Tsunami beyond the Vertical Revetment, PROCEEDINGS OF COASTAL ENGINEERING, JSCE, Volume 47, pp. 376-380 (in Japanese).
- https://www.jstage.jst.go.jp/article/proce1989/47/0/47_0_376/_pdf/-char/en
- Ports and Harbours Association of Japan (2007) Technical standard of the facilities and manuals of the harbor (in Japanese).
- <https://www.phaj.or.jp/cgi-bin/book/book.cgi?no=24&stock=>
- Rubey, W. W. (1933) Settling Velocity of Gravel, Sand and Silt Particles, American Journal of Science, Vol. 25, pp. 325-338.
- Sakakiyama, T., T. Yoshii, G. Shoji and S. Umetsu, (2011) Report of tsunami damage investigation by CRIEP team, 2011 Great East Japan Earthquake Tsunami Joint Survey Group Report Meeting, July 2011, pp. 77-82 (in Japanese).
- http://www.coastal.jp/files/tjtreport_20110716.pdf
- Sakakiyama, T. (2012) Tsunami Inundation Flow and Tsunami Pressure on Structures, Journal of JSCE, Ser. B2 (Coastal Engineering), Vol. 68, pp. 771-775 (in Japanese).
- https://www.jstage.jst.go.jp/article/kaigan/68/2/68_I_771/_pdf
- Shimazu, T., Y. Fukuhara, S. Arinaga, A. Matsuo, A. Nakayama and S. Tadehara (2001) Building Materials, Morikita Publishing Co., Ltd., ISBN 9784627551435, pp. 26-27 (in Japanese)
- Sugano, T. (2011) Port and Airport Research Institute, National Institute for Land and Infrastructure Management and Fisheries Research Agency, "Report of Investigation of Earthquake and Tsunami Damage to Ports, Harbors, Airports and Fishing Ports Due to the Great East Japan

- Earthquake”, Technical Lectures on Ports, Harbors, Airports and Fishing Ports.
<http://www.pari.go.jp/files/items/3649/File/4sugano2.pdf>
- Sugawara, D., H. Naruse and H. Goto, (2014) Numerical modeling of tsunami sediment transport considering energy dissipation due to sediment suspension, The Sedimentological Society of Japan, Proceeding, O27 (in Japanese).
<http://sediment.jp/04nennkai/2014/abstract.pdf>
- Sugawara, D. and T. Takahashi (2014) Numerical Simulation of Coastal Sediment Transport by the 2011 Tohoku-Oki Earthquake Tsunami, Advances in Natural and Technological Hazards Research, Vol. 35, pp. 99-112.
- Sugawara, D., T. Takahashi and F. Imamura (2014) Sediment transport due to the 2011 Tohoku-oki tsunami at Sendai: Result from numerical modeling, Marine Geology 358,
<http://dx.doi.org/10.1016/j.margeo.2014.05.005>, pp. 18-37.
- Suwa, Y.(2011) Great East Japan Earthquake Report Meeting, 2.4 Sea Coast, Characteristics of Damage to Coastal Structures and Hinterland from Tsunami (National Institute for Land and Infrastructure Management, Ministry of Land, Infrastructure, Transport and Tourism), April 2011 (in Japanese).
<http://www.nilim.go.jp/lab/bbg/saigai/h23tohoku/>
- Takabatake, D., N. Kihara and N. Tanaka, (2013) Numerical Study for the Hydrodynamic Pressure on the Front of Onshore Structures by Tsunami, Journal of JSCE, Ser. B2 (Coastal Engineering), Vol. 69, pp. 851-855 (in Japanese).
https://www.jstage.jst.go.jp/article/kaigan/69/2/69_I_851/_pdf
- Takabatake, D., N. Kihara, H. Kaida, Y. Miyagawa, A. Shibayama and M. Ikeno (2015) Development of tsunami fragility evaluation methods by large scale experiments (Part II) - Validation of the applicability of evaluation methods of impact force due to tsunami floating debris -, CRIEPI Research Report O15003 (in Japanese).
<http://criepi.denken.or.jp/jp/kenkikaku/report/download/4IwqvVnknASod9LgSHTWpiSOyQ71R2HX/O15003.pdf>
- Takahashi, S. (2011) Tsunami Damage in Ports, 2011 Great East Japan Earthquake Tsunami Joint Survey Group Report Meeting, July 2011, pp. 77-82 (in Japanese).
http://www.coastal.jp/files/tjtreport_20110716.pdf
- Takahashi, T., N. Shuto, F. Imamura and D. Asai (1999) A Movable Bed Model for Tsunamis with Exchange Rate between Bed Load Layer and Suspended Layer, Proceedings of Coastal Engineering, JSCE, Vol. 46, pp. 606-610 (in Japanese).
<http://library.jsce.or.jp/jsce/open/00008/1999/46-0606.pdf>
- Takahashi, T., T. Kurokawa, M. Fujita and H. Shimada (2011) Hydraulic Experiment on Sediment Transport due to Tsunamis with Various Sand Grain Size, Journal of JSCE, Ser. B2 (Coastal

- Engineering), Vol. 67, pp. 231-235 (in Japanese).
https://www.jstage.jst.go.jp/article/kaigan/67/2/67_2_I_231/_pdf
- Tamada, T., T. Tamura, T. Takahashi and Sasaki, H. (2009) Applicability of movable bed model for tsunami in tsunami disaster reduction in rivers, Journal of JSCE, Ser. B2 (Coastal Engineering), Vol. 65, pp. 301-305 (in Japanese).
https://www.jstage.jst.go.jp/article/kaigan/65/1/65_1_301/_pdf
- Tanimoto, K., H. Tsuruya and S. Nakano (1984) PROCEEDINGS OF THE JAPANESE CONFERENCE ON COASTAL ENGINEERING, Volume 31 (1984), pp. 257-261 (in Japanese). https://www.jstage.jst.go.jp/article/proce1970/31/0/31_0_257/_pdf/-char/en
- Tomita, T. (2011) Port and Airport Research Institute, National Institute for Land and Infrastructure Management and Fisheries Research Agency, “Report of Investigation of Earthquake and Tsunami Damage to Ports, Harbors, Airports and Fishing Ports Due to the Great East Japan Earthquake”, Technical Lectures on Ports, Harbors, Airports and Fishing Ports, (in Japanese) <http://www.pari.go.jp/files/items/3649/File/5tomita.pdf>
- Yamamoto, Y., N. Charusrojanadeck and K. Nariyoshi, (2011) Proposal of Rational Evaluation Methods of Structure Damage by Tsunami, Journal of Japan Society of Civil Engineers, Ser. B2 (Coastal Engineering), Volume 67 (2011) Issue 1, pp. 72-91 (in Japanese).
https://www.jstage.jst.go.jp/article/kaigan/67/1/67_1_72/_pdf/-char/en
- Yamashita, K., D. Sugawara, T. Takahashi, F. Imamura, Y. Saito, Y. Imato, T. Kai, H. Uehara, T. Kato, K. Nakata, R. Saka and A. Nishikawa (2015) Numerical Simulation of Large-Scale Sediment Transport Due to The 2011 Tohoku Earthquake Tsunami in Rikuzentakata City, Journal of JSCE, Ser. B2 (Coastal Engineering), Vol. 71, pp. 499-504 (in Japanese).
https://www.jstage.jst.go.jp/article/kaigan/71/2/71_I_499/_pdf
- Yasuda, T., T. Takayama and H. Yamamoto (2006) Characteristics of Deformations and Forces on Dispersive Solitons of Tsunami, Annual Journal of Coastal Engineering, JSCE, Vol. 53, pp. 256-260 (in Japanese).
<http://library.jsce.or.jp/jsce/open/00008/2006/53-0256.pdf>